Journal of Vertebrate Paleontology

ISSN: (Print) (Online) Journal homepage: www.tandfonline.com/journals/ujvp20

Hyracoidea from the Oligocene of Topernawi, Turkana Basin, Kenya

Natasha S. Vitek, Erik R. Seiffert, Steven Heritage, Margaret Wambui Gaiku, Craig S. Feibel, Francis J. Sousa, Isaiah O. Nengo, Eipa Emmanuel Aoron & Patricia M. Princehouse

To cite this article: Natasha S. Vitek, Erik R. Seiffert, Steven Heritage, Margaret Wambui Gaiku, Craig S. Feibel, Francis J. Sousa, Isaiah O. Nengo, Eipa Emmanuel Aoron & Patricia M. Princehouse (04 Nov 2024): Hyracoidea from the Oligocene of Topernawi, Turkana Basin, Kenya, Journal of Vertebrate Paleontology, DOI: 10.1080/02724634.2024.2409326

To link to this article: https://doi.org/10.1080/02724634.2024.2409326

Journal of Vertebrate Paleontology e2409326 (24 pages)

DOI: 10.1080/02724634.2024.2409326

ARTICLE

HYRACOIDEA FROM THE OLIGOCENE OF TOPERNAWI, TURKANA BASIN, KENYA

NATASHA S. VITEK,[1,2*] ERIK R. SEIFFERT,[3,4,5] STEVEN HERITAGE,[3,4] MARGARET WAMBUI GAIKU,[6] CRAIG S. FEIBEL,[7] FRANCIS J. SOUSA,[8] ISAIAH O. NENGO,[2‡] EIPA EMMANUEL AORON,[6,9] and PATRICIA M. PRINCEHOUSE[10,11]

[1]Department of Ecology & Evolution, Stony Brook University, Stony Brook, New York 11794-5245, U.S.A., natasha.vitek@stonybrook.edu;
[2]Turkana Basin Institute, Stony Brook University, Stony Brook, New York 11794-4364, U.S.A.;
[3]Department of Integrative Anatomical Sciences, Keck School of Medicine of USC, Los Angeles, California 90033, U.S.A., seiffert@usc.edu, steven.heritage@usc.edu;
[4]Duke Lemur Center Museum of Natural History, 1013 Broad Street, Durham, North Carolina 27705, U.S.A.;
[5]Department of Mammalogy, Natural History Museum of Los Angeles County, Los Angeles, California 90007, U.S.A.;
[6]Department of Biological and Physical Sciences, Turkana University College, Lodwar, 3J88+5WP, Kenya, gaikumargaret@gmail.com;
[7]Department of Earth and Planetary Sciences, Rutgers University, New Brunswick, New Jersey 08901, U.S.A., feibel@eps.rutgers.edu;
[8]College of Earth, Ocean, and Atmospheric Sciences, Oregon State University, Corvallis, Oregon 97331, U.S.A., francis.sousa@oregonstate.edu;
[9]Department of Human Evolutionary Biology, Harvard University, Cambridge, Massachusetts 02138, U.S.A., eaoron@g.harvard.edu;
[10]Institute for the Science of Origins, Case Western Reserve University, Cleveland, Ohio 44106, U.S.A.;
[11]Anthropology Department, SUNY Oswego, Oswego, New York 13126, U.S.A., patricia.princehouse@oswego.edu

ABSTRACT—The Topernawi area of west Turkana, northern Kenya, preserves a number of recently discovered vertebrate fossil localities of mid-Oligocene age. The Topernawi fauna provides important new data on mammalian evolution in equatorial eastern Africa during the mid-Cenozoic. Here, we describe five new species of hyracoids from Topernawi: *Nengohyrax josephi*, *Abdahyrax philipi*, *Geniohyus ewoii*, *Thyrohyrax lokutani*, and *Thyrohyrax ekaii*. These species range in reconstructed body mass from ~8 to ~150 kg, comparable to the body size range that has been observed at other hyracoid-rich Paleogene sites. We use Bayesian tip-dating phylogenetic analyses to estimate hyracoid relationships. We find that non-*Thyrohyrax* species from Topernawi are members of Geniohyidae, a clade of bunodont, Paleogene hyracoids. Despite being approximately the same age as some of the youngest and best-sampled horizons in the Jebel Qatrani Formation (Fayum, northern Egypt), the Topernawi hyracoid fauna is distinct, and shows no overlap at the species level; it also shows no species overlap with the ~1.5–2.5 Ma younger Chilga localities in northern Ethiopia. The hyracoid assemblage from Topernawi adds to a growing body of evidence which suggests that certain distinctive clades known from earlier Oligocene horizons in northern Africa (*Saghatherium*, *Selenohyrax*, *Titanohyrax*) did not persist into the late Oligocene.

http://zoobank.org/urn:lsid:zoobank.org:pub:D2F3578A-6153-481B-BEC4-A8007B7DC606

SUPPLEMENTARY FILES—Supplementary files are available for this article for free at www.tandfonline.com/UJVP.

Citation for this article: Vitek, N. S., Seiffert, E. R., Heritage, S., Gaiku, M. W., Feibel, C. S., Sousa, F. J., Nengo, I. O., Aoron, E. E., & Princehouse, P. M. (2024) Hyracoidea from the Oligocene of Topernawi, Turkana Basin, Kenya. *Journal of Vertebrate Paleontology.* https://doi.org/10.1080/02724634.2024.2409326

Submitted: September 11, 2023
Revisions received: August 22, 2024
Accepted: September 3, 2024

INTRODUCTION

Hyracoids are afrotherian mammals that once formed a dominant component of terrestrial mammalian faunas in Africa and Arabia (Rasmussen, 1989; Rasmussen & Gutierrez, 2009; Stanhope et al., 1998). Today, their diversity consists of at least five species of relatively small, and closely related, terrestrial and arboreal hyraxes (Hoeck, 2011; Huxley, 1869; IUCN, 2022; Oates et al., 2022). In the Paleogene, hyracoids were much more diverse, with multiple species ranging in size from ~8 to ~1000 kg in a single community (Schwartz et al., 1995).

The reference point for Paleogene hyracoid diversity has long been the Eocene and Oligocene localities of the Fayum Depression in Egypt, which were the only pre-Miocene sites with a large, well-studied sample of hyracoids in the 20th century (Barrow et al., 2010, 2012; De Blieux & Simons, 2002; Rasmussen, 1989; Rasmussen et al., 1990; Rasmussen & Simons, 1988, 1991, 2000; Thewissen & Simons, 2001). In the last three decades, additional fossils of Paleogene hyracoids have been documented from Algeria (Benoit et al., 2016; Court

*Corresponding author.
‡Deceased.

Published online 04 Nov 2024

& Mahboubi, 1993; Tabuce et al., 2001), Angola (Tabuce et al., 2021), Ethiopia (Kappelman et al., 2003), Kenya (Ducrocq et al., 2010; Rasmussen & Gutierrez, 2009), Libya (Coster et al., 2015; Thomas et al., 2004), Namibia (Pickford et al., 2008), Oman (Pickford, 1994), Tanzania (Stevens et al., 2009), and Tunisia (Court & Hartenberger, 1992). These additions to the Afro-Arabian hyracoid record suggest a Paleogene history of high species richness and local endemism that cannot be sufficiently characterized by any single fauna.

In particular, Oligocene records from eastern Africa are important for understanding a major transition in hyracoid diversity between the Paleogene and Neogene. The primary interval of diversity loss in hyracoids occurred by the Early Miocene, in association with faunal interchange between Afro-Arabia and Eurasia (Kappelman et al., 2003; Rage & Gheerbrant, 2020; Rasmussen & Gutierrez, 2009). This Early Miocene record is represented in several Kenyan sites (Leakey et al., 2011; Lukens et al., 2017; Whitworth, 1954). In contrast, pre-interchange Oligocene sites in eastern Africa are scarce, principally including the Ethiopian Chilga site and three Kenyan sites: Lokone, Losodok (Lothidok), and Nakwai (Ducrocq et al., 2010; Kappelman et al., 2003; Rasmussen & Gutierrez, 2009).

Here, we describe specimens of Hyracoidea from Topernawi, an area with several newly discovered mid-Oligocene vertebrate fossil localities located approximately 25 km to the west of Lake Turkana. The Topernawi localities are notable for being dominated by hyracoid fossils. Members of this order comprise almost 75% of identified specimens. In addition to recognizing the Topernawi hyracoids as new species, we add them to an existing character-taxon matrix to estimate evolutionary relationships with other living and extinct members of Hyracoidea using Bayesian tip-dating. We also estimate the body size of species from Topernawi as a first-order approximation of ecological diversity of hyracoids within the site (Schmidt-Nielsen, 1984; Schwartz et al., 1995).

Geological Context

Topernawi is located in the western part of the Turkana Depression approximately 25 km west of Lake Turkana in Turkana County, Kenya (Fig. 1). Fossiliferous deposits are part of the Topernawi Formation, exposed in the Ekitale Basin, which currently crops out over an area limited to a few square kilometers (Ragon et al., 2019; Sousa et al., 2022). The formation records an episode of pyroclastic deposition and reworking across a low-relief landscape. The initial description of these strata by Ragon et al. (2019) described a 75 meter succession, which they subdivided into five units (U1 to U5). ^{40}Ar-^{39}Ar geochronology provides tight bracketing ages that constrain the depositional age of the fossiliferous deposits of the Topernawi Formation. A columnar jointed basaltic lava flow immediately beneath the basal Topernawi Formation yields an age of 29.7 ± 0.5 Ma (2σ), and a welded ignimbrite near the top of the section is dated at 29.24 ± 0.08 Ma (2σ) (Sousa et al., 2022). These dates constrain the depositional age of the fossiliferous units in the Topernawi Formation to be deposited between 30.2 and 29.16 Ma (2σ). These rocks represent the oldest dated synrift sedimentary section in the western Turkana Depression.

Vertebrate fossils from Topernawi were first found in 2019 as part of field surveys conducted by the Topernawi Research Project. Within the Topernawi Formation, the majority of hyracoid fossils come from two stratigraphic units. These units, U3 and U4, are primary and reworked volcaniclastic sedimentary deposits. Unit 3 is dominated by meter-scale tabular beds of volcaniclastic sand to gravel, frequently reworked by decameter-wide channels, and U4 is also composed of reworked volcaniclastic sediments, locally showing evidence for ballistic pyroclastic processes and airfall accumulation (Ragon et al., 2019).

The majority of fossils are preserved in a well-identified stratigraphic zone circa 3–4 m thick near the U3/U4 conformity (Fig. 1). Fossils are most frequently found in a silty sandstone bed that we interpret as a reworked volcaniclastic lithology. The mild reworking of volcaniclastic sediments in the fossil-bearing strata, and the lack of articulated fossils in those beds, suggests that the process that brought the fossils to the location we find them today involved some physical movement (reworking) along with their volcaniclastic host sediments. This reworking obfuscates direct evidence for the paleoenvironment in which the fossil organisms lived. However, the significant number of well-preserved tooth fossils with complete crowns and minimal abrasion (Baczynski et al., 2016; Behrensmeyer, 1975; Moore & Norman, 2009) suggests that the extent of reworking and distance traveled must have been limited, inconsistent with the kind of taphonomic transport damage expected from initial transport and deposition, re-excavation from scouring, and subsequent further transport that would be expected of reworking of sediments deposited elsewhere prior to the deposition of U3. Pedogenic modification of the sediments is extremely minimal, but leaf impressions are preserved on clay laminae near the U3/U4 contact.

Institutional Abbreviations—**AMNH**, American Museum of Natural History, New York, NY, U.S.A.; **DPC**, Duke Lemur Center Museum of Natural History, Duke University, Durham, NC, U.S.A.; **KNM**, Kenya National Museums, Nairobi, Kenya; **UMZC**, University Museum of Zoology, Cambridge, U.K.; **YPM**, Yale Peabody Museum, New Haven, CT, U.S.A.

Anatomical Abbreviations—Terminology primarily comes from Barrow et al. (2010) and Rasmussen and Simons (1988), with additions where indicated in Figure 2 (Pickford, 2004). We consider the cristae/ids to be homologous to loph/ids described in other hyracoid taxa (for example, protocristid vs. protolophid). We use the former term instead of the latter because in the specimens described here, these structures are not always continuous in all described taxa, and therefore -crista/-cristid is the more conservative term that can be applied to all species.

MATERIALS AND METHODS

Fossil Identification

Very few teeth from Topernawi are associated. Therefore, identification of teeth to species as well as tooth position required some inference that we detail here. First, we separately studied the lower molars, then the upper molars, to group them into broad morphotypes. Similarity in size and similarity in overall morphological features served as grouping criteria.We assumed that certain features of crown topology, such as the appression of cusps or the degree to which two cusps on the crown are located close together, were more likely to be similar within a species than between species, based on developmental and quantitative genetic studies supporting a model of significant shared underlying genetic patterning between metameres in a dental field (Hlusko et al., 2016; Koh et al., 2010). To avoid confusion of different metameres for different species in this qualitative step, we minimized reliance on features that we observed to vary between serial homologues in better-known hyracoid taxa, such as the position of the parastyle (e.g., *Pachyhyrax crassidentatus*, DPC 4000), or overall length and width proportions (Seiffert, 2007).

At this stage, we did not require upper and lower molars to group into the same number of morphotypes in order to allow each set of molars to be investigated independently. However, after this step was completed, if we found that each morphotype was reasonably abundant among upper teeth, then it was reasonable to hypothesize that each should be represented at least once in the collection of lower teeth and vice versa. Therefore, we expected comparative study of upper and lower molars to converge on the same number of morphotypes; this convergence

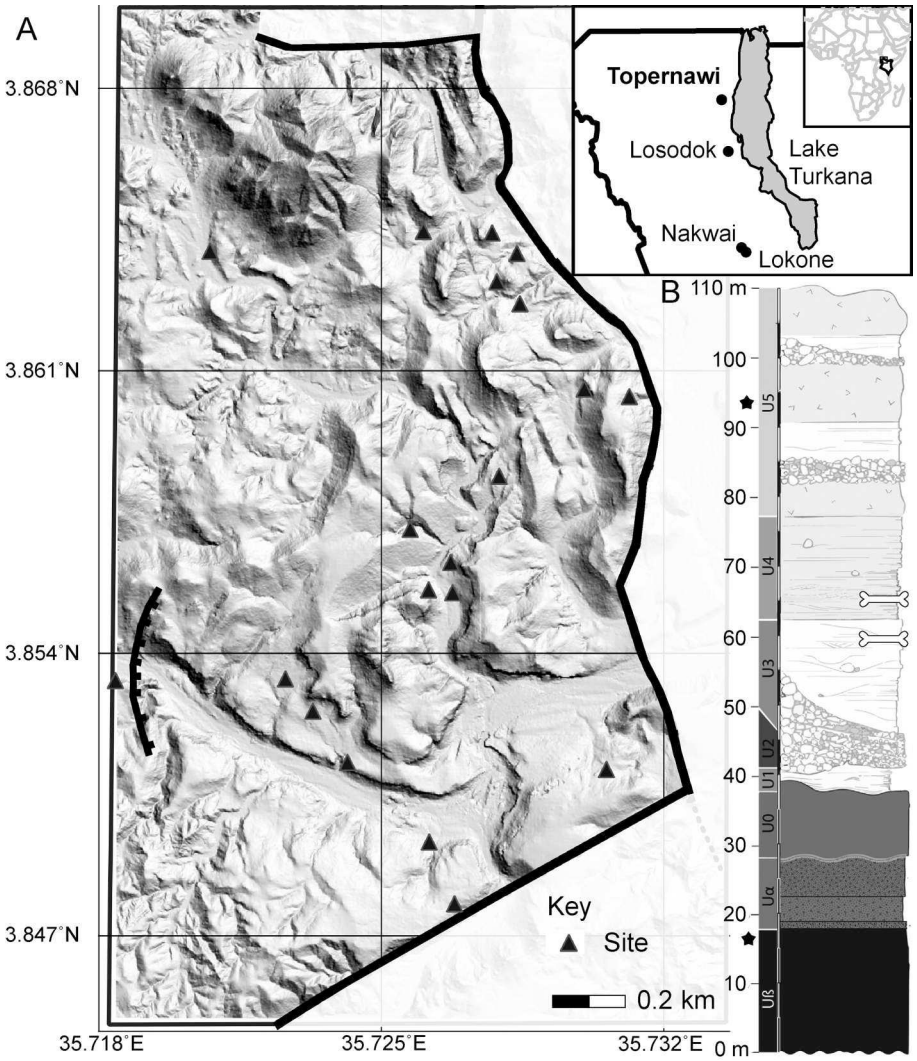

FIGURE 1. Geographic and geological summary of the Oligocene fossil site Topernawi in the Turkana region of Kenya. **A**, map of major fossil localities in Topernawi in relation to remote-sensing-based mapping of Ragon et al. (2019), draped over a digital elevation model (DEM) of the region. Inset shows map of the location of Topernawi in relation to other nearby late Oligocene and Early Miocene fossil sites in the Lake Turkana region of Kenya. Heavy black lines and lighter shading indicate the extent of the field area. **B**, stratigraphic section summarizing major lithological units within Topernawi. Stratigraphic section reproduced under a CC-BY license from Sousa et al. (2022). Stars indicate the stratigraphic levels of two radioisotopic dates. Bones indicate the main horizons from which vertebrate fossils were recovered.

occurred. After molar morphotypes were stabilized, we conducted additional comparative work to associate premolars with molar morphotypes based on size and similarity in features.

Then, we used previously proposed diagnostic differences in proportions to separate molar positions within a morphotype and between metameres (Butler, 1939; Novacek et al., 1985; Seiffert, 2007; Vitek & Princehouse, 2024). To help assign tooth positions of lower molars, we used the talonid width relative to trigonid width as well as tooth size relative to teeth assigned to m1 (Fig. 3). For premolars, we made the assumption that teeth increased in size along the premolar field mesiodistally, matching observations in hyracoid taxa with associated dentitions (e.g., Asher et al., 2017; Barrow et al., 2012; Rasmussen & Simons, 1988). For upper molars, we primarily used relative size (see Supplementary Information, Fig. S1), distinctive features common to hyracoid M3s such as closely appressed hypoconid and metaconid with an expanded distocrista, and, where applicable, features observed to metamerically vary in other taxa, such as the position of the parastyle (Seiffert, 2007). To facilitate future independent evaluations of our resulting identifications, we present illustrations of upper and lower teeth, with the exception of deciduous teeth, in a matrix-like format where species are in rows and tooth positions are in columns, with each species-specific position represented by two teeth where possible to illustrate variation (Figs. 4–6). Isolated teeth with ambiguous combinations of size and features were not assigned a particular position, although these specimens are relatively few, and in most cases ambiguity was due to wear or significant specimen damage rather than transport. As an additional check on our associations of specimens and evaluation of serial homologs, we provide relative crown areas and coefficients of variation of crown size in the context of other, more completely known species from a previously published dataset (see Supplementary Information Figs. S2, 3; Vitek & Princehouse, 2024).

Finally, we associated upper and lower teeth based on similarity in size and morphological characters where applicable. Our expectation was that associated upper and lower teeth should share a size range and morphological arrangement of cusps and crests that would permit precise occlusion (Crompton & Hiiemae, 1970; Marshall & Butler, 1966). Notably, all but the smallest two taxa differ distinctly in absolute size, and it was logical to group the largest upper molar morphotype with the largest lower molar morphotype, etc. Supplementary features were consistent with this pairing. In one example, of all morphotypes in the collection the medium-sized morphotype (here described as *Geniohyus ewoii*) has the least strongly expressed crests on both upper and lower molars. In a second example, the relatively short trigonid basin of the second-largest lower

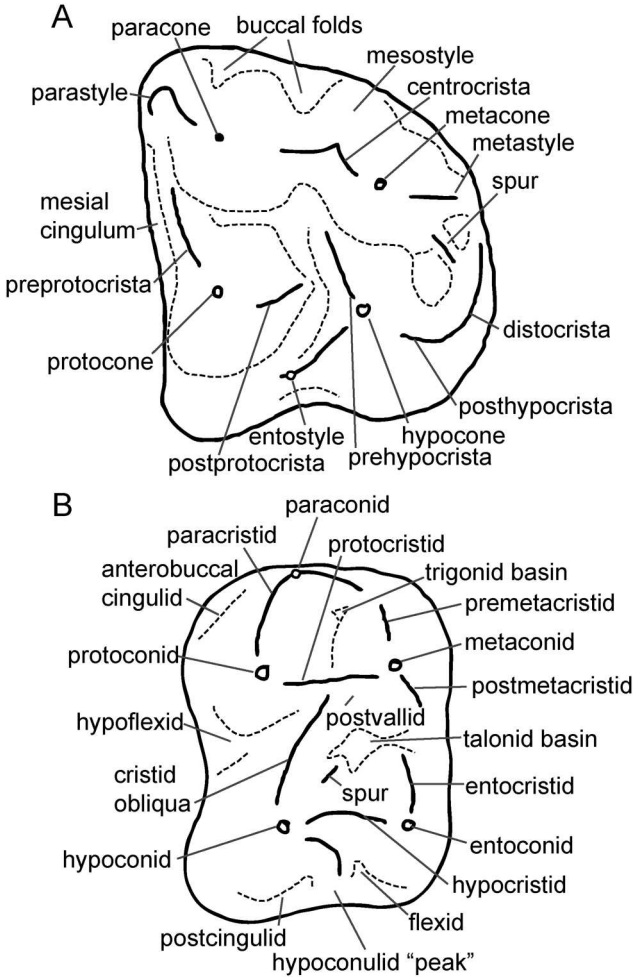

FIGURE 2. Dental terminology diagram illustrating features of upper and lower hyracoid tooth crowns described in this work. **A**, upper left M3, anterior is to the left. **B**, lower left m2, anterior is to the top of the image. Line drawings are amalgamations of different specimens combined to illustrate all terms.

molar morphotype (here described as *Abdahyrax philipi*) should correspond to a relatively more closely appressed paracone and metacone in comparison to other morphotypes to facilitate precise occlusion. The second-largest upper molar morphotype has, correspondingly, a relatively mesiodistally compressed tooth with a relatively shorter distance between the paracone and metacone relative to the largest upper molar morphotype. As an additional check on associations of upper and lower molars, we evaluated whether upper and lower teeth had relative proportions similar to those of more completely known species. This visual evaluation was accomplished by plotting proportions of corresponding teeth (e.g., m1 vs. M1) in morphotypes from Topernawi and those of other species known from more complete remains from a previously published dataset (see Supplementary Information, Fig. S4; Vitek & Princehouse, 2024).

Phylogenetic Analyses

We developed a character-taxon matrix based on that in Cooper et al. (2014), which is derived from Barrow et al. (2010, 2010, 2012), Seiffert (2007), and Seiffert et al. (2012). We subsequently modified it in Mesquite 3.70 (Maddison & Maddison, 2021). All species were removed from the dataset except for hyracoids and three early afrotherian taxa retained as outgroups, *Ocepeia daouiensis*, *Eritherium azzouzorum*, and *Phosphatherium escuilliei*. The five new hyracoid species from Topernawi were added. Ten additional dental characters were added because they helped differentially diagnose taxa from Topernawi and were hypothesized to be phylogenetically informative among hyracoids. A list of specimens and images from the literature used to score existing taxa for these new characters is included in Supplemental Data (Asher et al., 2017; Barrow et al., 2010; Benoit et al., 2016; Court & Mahboubi, 1993; Gheerbrant, 2009; Gheerbrant et al., 2005, 2014; Kocsis et al., 2014; Matsumoto, 1921; Pickford, 1994, 2019; Pickford et al., 2008; Rasmussen & Gutierrez, 2010; Rasmussen & Simons, 1988, 1991; Seiffert, 2006; Tabuce, 2016; Tabuce et al., 2001; Yans et al., 2014) . The final character matrix contained 33 taxa and 413 characters. Of those characters, 172 were invariant and 57 were autapomorphic, or parsimony uninformative.

In the original version of the matrix, polymorphic characters were given unique character states, resulting in some characters that had up to 20 character states (Seiffert, 2007). We revised characters to treat polymorphic scores as the more standard combination of two or more character states, resulting in a smaller number of character states that could be accommodated by the MrBayes analytical software (Ronquist et al., 2012). Characters were equally weighted, and all characters that formed plausible morphoclines were ordered following prior practice (Cooper et al., 2014). Additional edits to the matrix are as follows. The scores for upper teeth of *Microhyrax lavocati* were removed because the fossils on which these scores were based do not belong to this species (Tabuce & Benoit, 2014). Scores of lower premolars of *Titanohyrax angustidens* were based on deciduous teeth, so these scores were removed until observations are clarified. A Mesquite-readable nexus file including taxa, character scorings, character state descriptions, and decisions about character ordering is included in Supplemental Data. An online-accessible version of the NEXUS file is hosted on MorphoBank under project P4786 (http://morphobank.org/permalink/?P4786).

Absolute ages of extinct species were modeled as age ranges drawn from the literature in combination with the geological time scale (Barido-Sottani et al., 2020; Walker et al., 2019). The age ranges used and the sources for each estimate are provided in Supplemental Data (Barrow et al., 2010; Coster et al., 2012; Cote et al., 2018; Drake et al., 1988; Feibel & Brown, 1991; Gheerbrant, 2009; Gheerbrant et al., 2005, 2014; Heritage et al., 2021; Heritage & Seiffert, 2022; Kocsis et al., 2014; Leakey et al., 2011; Mahboubi et al., 1986; Matsumoto, 1921, 1926; Michel et al., 2020; Pickford, 1994, 2009; Pickford et al., 2008; Rasmussen & Gutierrez, 2010; Rasmussen & Simons, 1988, 1991, 2000; Seiffert, 2003, 2006; Sousa et al., 2022; Sudre, 1979; Tsujikawa & Pickford, 2006; Yans et al., 2014). The age of the root, which in this case models the origin of crown Afrotheria, was modeled as a half-normal distribution with a minimum age of 60.1 Ma and 99.7% tail within 70.1 Ma (Heritage et al., 2021; Heritage & Seiffert, 2022).

Bayesian phylogenetic analyses were run in the MrBayes v. 3.2.6 parallel (MPI) version (Ronquist et al., 2012). These analyses were time-scaled using tip dates to help inform the parameters of a fossilized birth-death (FBD) model (Heath et al., 2014). The probability of sampling species was set to 16.7% based on the proportion of extant hyracoid species sampled (Gavryushkina et al., 2016; Zhang et al., 2016). The clock rate prior was set as an approximately flat distribution. The three outgroups were enforced by setting a topological constraint. Each analysis was run for 50 million generations using two runs of four chains each, one cold chain and three hot chains with temperature set to 0.02. Chains were sampled every 1000 generations.

Two separate Bayesian analyses were conducted to account for the potential impact of the large number of invariant characters

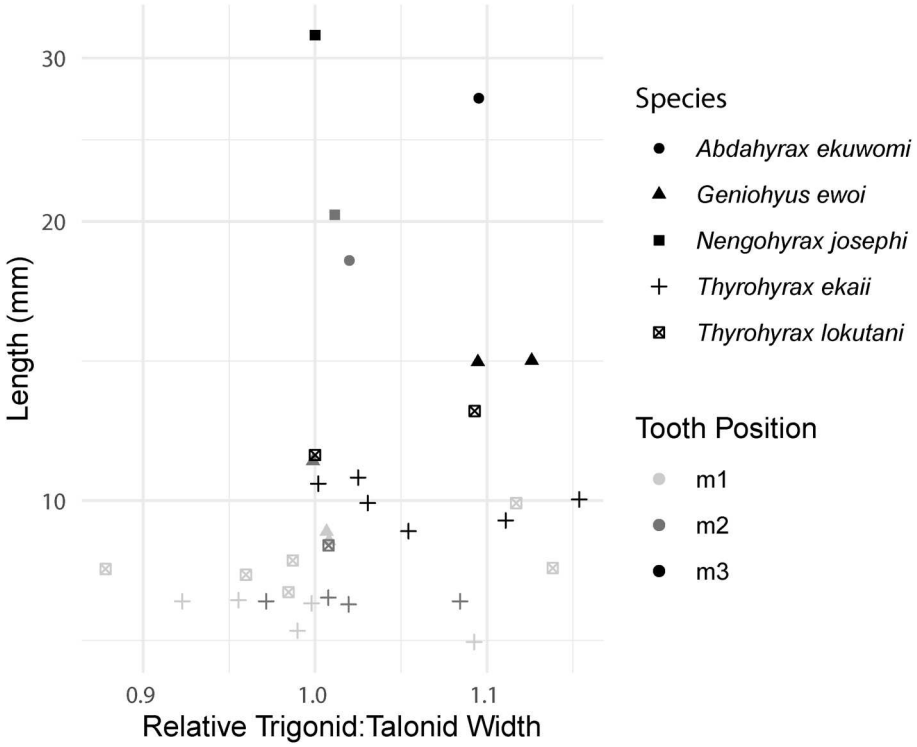

FIGURE 3. Plot of ratio values that help diagnose hyracoid lower molar loci. Ratios were measured in molars from Topernawi. Alongside information from associated dentitions, they were used to help evaluate which isolated teeth belonged to which tooth position for each species.

in our matrix of morphological characters. The two analyses differ only in modeling how the characters were sampled, and are otherwise identical in all settings. The first analyses implemented the gamma-distributed Markov k (Mk) model by setting coding to the default 'all' (Lewis, 2001). The second implemented the Markov k with ascertainment bias (Mkv) model by setting coding to 'variable.'

For each analysis, adequate sampling was checked in Tracer (Rambaut et al., 2018), using the criterion of effective sample size (ESS) > 200 as a threshold for adequate convergence as well as visual inspection of diagnostic plots (Drummond et al., 2006). Topological convergence between the two independent runs was checked using the average standard deviation of split frequencies, which was considered adequate if < 0.01. The first 25% of the sample was discarded as burn-in. The post-burn-in sample of topologies was summarized as a 50% consensus tree with Bayesian posterior probability (BPP) values indicating support for each node using the 'ggtree' package (Wang et al., 2020; Yu, 2022).

To complement Bayesian analyses, a parsimony analysis using implied weighting was conducted in TNT version 1.5 (Goloboff & Catalano, 2016). The default implied weighting value of K = 3 was maintained because it balanced being higher than values at which K shows undesirable properties in simulations (K < 2) while remaining as low as reasonably possible to avoid being redundant with equal-weights parsimony (M. R. Smith, 2019). We provide results of Bayesian analyses in the main text, but also include results of parsimony with implied weighting analysis in supplementary text to permit comparison as well as an initial assessment of which relationships are robust to analytical model choice. Scripts used to conduct analyses and summarize results are reposited in an associated project on Dryad.

Body Mass Estimates

To estimate the body mass of each new taxon, we used regression equations predicting mass from upper and lower m2 lengths of perissodactyls and hyracoids (Janis, 1990). Among other published models, this one is preferred for estimating hyracoid body size (Schwartz et al., 1995). We used the quasi-maximum likelihood estimator correction factor to correct for bias in detransformed logarithmic variables (R. J. Smith, 1993). We include estimates based on all available, identifiable second molars as well as including uncertainty within the model itself through the 95% confidence intervals.

SYSTEMATIC PALEONTOLOGY

MAMMALIA Linnaeus, 1758
AFROTHERIA Stanhope et al. 1998
HYRACOIDEA Huxley, 1869
GENIOHYIDAE Andrews, 1906

Type Genus—*Geniohyus*

Included Taxa—*Abdahyrax* gen. nov., *Brachyhyrax*, *Bunohyrax*, *Geniohyus*, *Nengohyrax* gen. nov., *Pachyhyrax*.

Emended Diagnosis—Apomorphies of Geniohyidae: presence of four roots on P1; presence of small metacone on P2; presence of posthypocrista on upper molars; presence of entostyle on upper molars; mesiobuccally inflated hypoconid on lower molars.

Remarks—Geniohyidae was previously characterized as a group of dentally primitive taxa including *Seggeurius*, *Geniohyus*, *Bunohyrax*, *Pachyhyrax*, and *Brachyhyrax* (Rasmussen & Gutierrez, 2010). With the exception of *Seggeurius*, the monophyly of this group has stood up to repeated phylogenetic assessments of relationships in parsimony analyses (Barrow et al., 2010; Cooper et al., 2014; Seiffert, 2007) as well as Bayesian analyses (this study). We formally recognize apomorphies, rather than plesiomorphic or primitive characters, that diagnose this clade based on phylogenetic analysis. Although many geniohyids have simplified premolars in terms of lower premolars lacking entoconids and upper molars having small hypocones, not all

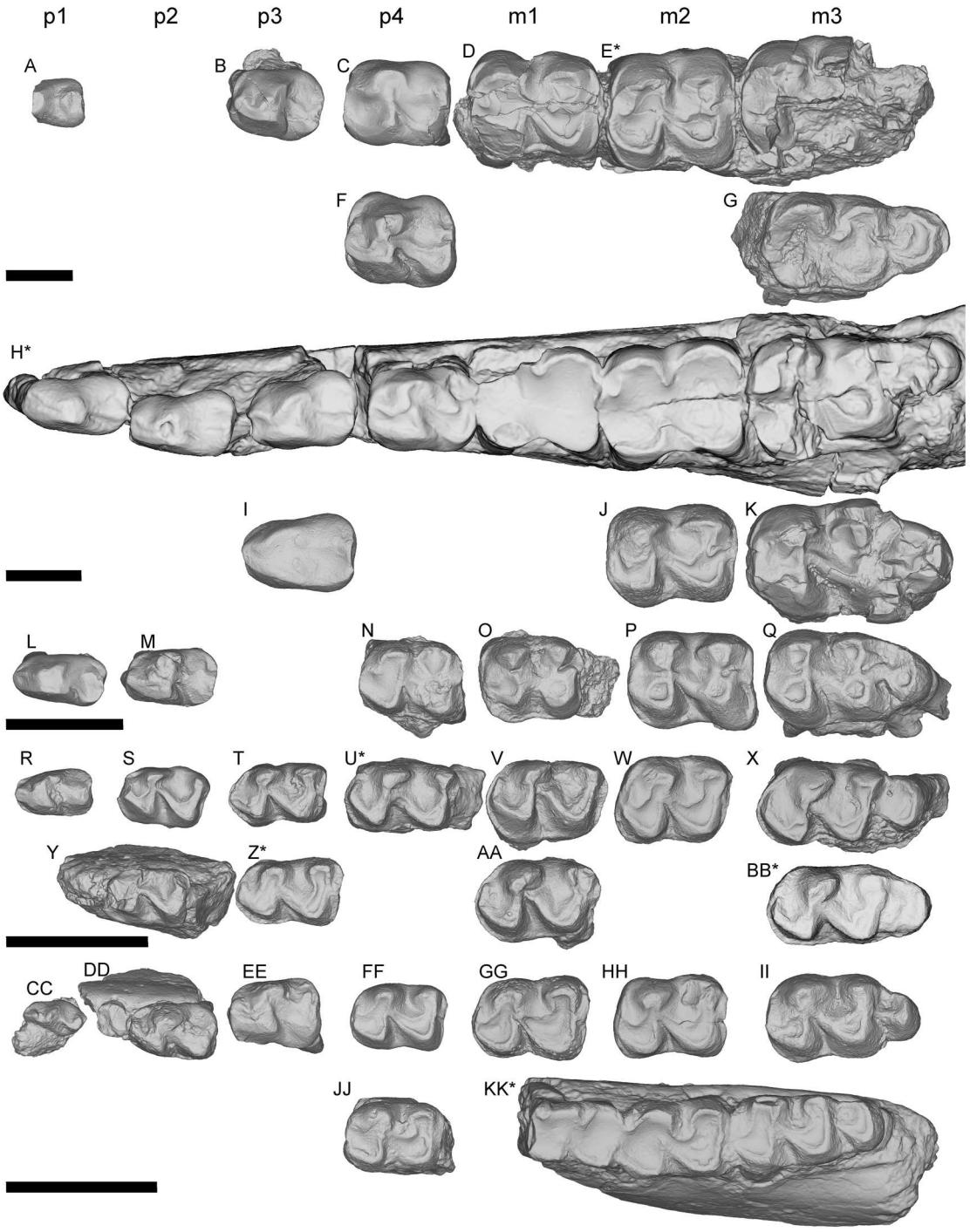

FIGURE 4. Lower teeth of hyracoids from Topernawi in occlusal view. Anterior is to the left. Images are organized by tooth position in columns. Some specimen images have been reversed as indicated to facilitate comparisons between taxa and tooth positions. **A**–**G**, *Nengohyrax josephi*. **A**, KNM-TP 102150, left p1; **B**, KNM-TP 102171, left p3; **C**, KNM-TP 102162, right p4 (reversed); **D**, KNM-TP 102109, left m1; **E**, KNM-TP 102172, holotype, left m2 and partial m3; **F**, KNM-TP 102487, right p4 (reversed); **G**, KNM-TP 102739, right m3 (reversed). **H**–**K**, *Abdahyrax philipi*. **H**, KNM-TP 102936, holotype, left p1–m3; **I**, KNM-TP 102207 right p3 (reversed); **J**, KNM-TP 102214 left m2; **K**, KNM-TP 102114, left m3. **L**–**Q**, *Geniohyus ewoii*. **L**, KNM-TP 102459, left p1; **M**, KNM-TP 102186, left p2; **N**, KNM-TP 102527, left p4; **O**, KNM-TP 102104, left m1; **P**, KNM-TP 102518, right m2 (reversed); **Q**, KNM-TP 102465, left m3, **R**–**BB**; *Thyrohyrax lokutani*. **R**, KNM-TP 102158, right p1 (reversed); **S**, KNM-TP 102163, right p2 (reversed); **T**, KNM-TP 102528, left p3; **U**, KNM-TP 102526 (in part), holotype, right p4 (reversed); **V**, KNM-TP, 102464, left m1; **W**, KNM-TP 102142, left m2, **X**, KNM-TP, 102463, left m3; **Y**, KNM-TP, 102130, left p2; **Z**, KNM-TP 102526 (in part), holotype, left p3; **AA**, KNM-TP 102504, left m1; **BB**, KNM-TP 102526 (in part), holotype, left m3. **CC**–**KK**, *Thyrohyrax ekaii*. **CC**, KNM-TP 102513, left p1; **DD**, KNM-TP 102225, right p2 (reversed); **EE**, KNM-TP 102180, left p3; **FF**, KNM-TP 102235, left p4; **GG**, KNM-TP 102456, left m1; **HH**, KNM-TP 102237, left m2; **II**, KNM-TP 102204, left m3; **JJ**, KNM-TP 102250, left p4; **KK**, KNM-TP 102173, holotype, left dentary with m1–m3. Scale bars equal 1 cm. Codes at top indicate columns of tooth positions. Asterisk indicates a holotype.

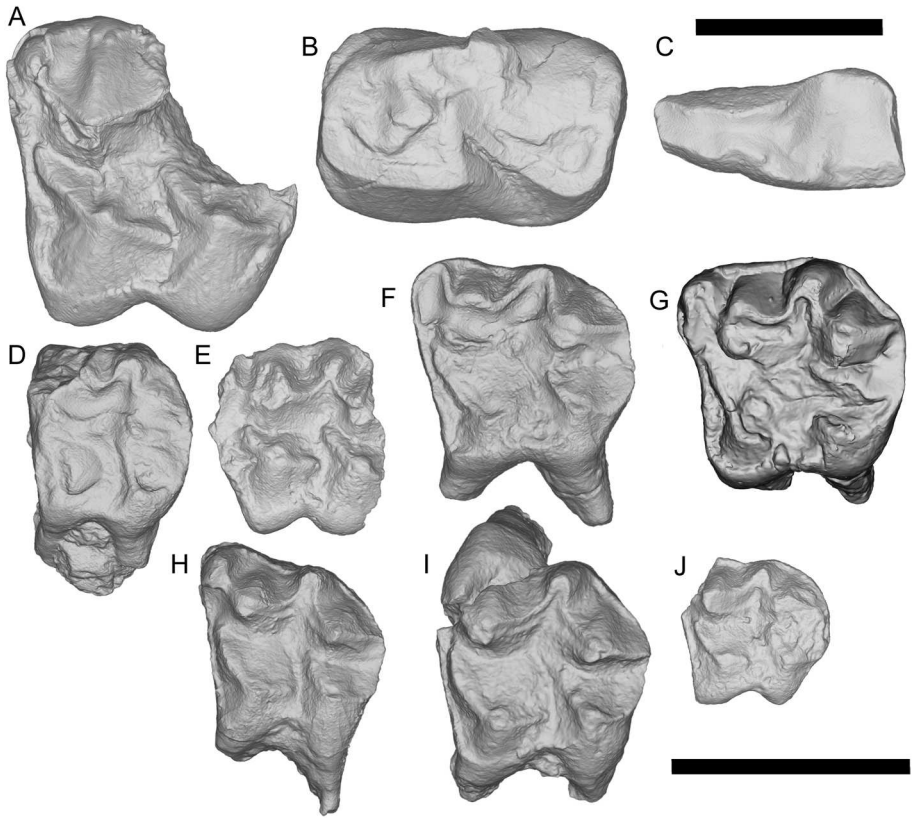

FIGURE 5. Deciduous teeth of hyracoids from Topernawi in occlusal view. Anterior is to the left. Some specimen images have been reversed as indicated to facilitate comparisons between taxa and tooth positions. **A**, KNM-TP 102177, left dP4; **B**, KNM-TP 102510, right dp4 (reversed); **C**, KNM-TP 102228 left dp2; **D**, KNM-TP 102202, left dP3; **E**, KNM-TP 102157, left dP4; **F**, KNM-TP 102187, left dP4; **G**, 102831 (in part), left dP4; **H**, KNM-TP 102147, left dP4; **I**, KNM-TP 102501, left dP4; **J**, KNM-TP 102261, right dP3 (reversed). Scale bars equal 1 cm. The scale bar at top applies to **A**–**C**. The scale bar at bottom applies to **D**–**J**.

taxa share these traits and therefore we do not include them in the diagnosis.

NENGOHYRAX JOSEPHI gen. et sp. nov.
(Figs. 4, 5, and 6; Table 1)

Holotype—KNM-TP 102172, left dentary fragment with m2 and a fragment of m3 (Fig. 4E).

Etymology—Genus named for Isaiah Nengo, who was instrumental in conducting early work at the site; species named for Joseph Lokutan, who found the type specimen.

Referred Specimens—KNM-TP 102081 right P4, KNM-TP 102086 right m1, KNM-TP 102103 left P4, KNM-TP 102105 left M3, KNM-TP 102109 right m1, KNM-TP 102110 left M3, KNM-TP 102113 left m2, KNM-TP 102150 left p1, KNM-TP 102156 left M1 or M2, KNM-TP 102162 left p4, KNM-TP 102165 right M2, KNM-TP 102171 left p3, KNM-TP 102172 left m2, KNM-TP 102174 right P1, KNM-TP 102177 left dP4, KNM-TP 102190, left M2, KNM-TP 102193 left M2, KNM-TP 102208 left M3, KNM-TP 102244 left P2, KNM-TP 102458 right P3, KNM-TP 102467 left P1, KNM-TP 102468 right P2, KNM-TP 102475 right P4, KNM-TP 102481 right P2, KNM-TP 102484 left P3, KNM-TP 102487 right p4, KNM-TP 102489 left upper premolar, KNM-TP 102490 left M1, KNM-TP 102491 left P2, KNM-TP 102510 right dp4, KNM-TP 102522, right P4, KNM-TP 102739, right m3.

Diagnosis—Apomorphies within Geniohyidae: spurs in trigonid basin absent; molar prehypocrista terminates along mesial wall of metacone. Differs from other geniohyids in combination of: incipient p4 protolophid; molar trigonids enclosed by paracristid and premetacristid; absence of hypocones on premolars.

Description

Upper Premolars— The dentition increases distally in size, from premolars to molars. Teeth are brachydont. The premolars have weak or absent mesiobuccal cingula and lack hypocones. The lingual part of the crown consists of a protocone with a preprotocrista ending at the mesial cingulum with a distinct cuspule that may be a paraconule along its length. The postprotocrista extends into a broad, flat shelf devoid of any cuspule or ridge that might indicate a hypocone. The P1 (KNM-TP 102467, KNM-TP 102489; Fig. 6A, H) has four roots and a relatively small protocone. The paracone and metacone are closely appressed, connected by a crista that continues in a straight line through a postmetacrista. A parastyle approximately half the size of the paracone is present. The P2 (KNM-TP 102468, KNM-TP 102244; Fig. 6B, I) also has four roots, but a larger protocone than the P1. It is buccolingually wider than the P1 with more distinct separation between the paracone and metacone. Buccal cingula are variably present and discontinuous. P3s (KNM-TP 102484, KNM-TP 102458; Fig. 6C, J) are similar to P2s but larger in size and with a more strongly expanded distolingual surface. P4s (KNM-TP 102475; Fig. 6D) are much wider than long, in comparison to the more equilateral dimensions of anterior premolars.

One partial upper cheek tooth (KNM-TP 102177; Fig. 5A) is smaller than other identified molars of this species, but otherwise shares several anomalous features, including a cuspule on the mesial cingulum anteromesial to the protocone, strong cristae on the protocone oriented approximately continuously with each other, and a distal continuation of the mesiolingual cingulum that travels up the lingual face of the hypocone. The crown is proportionally narrower than P4s (Table 1). We infer that

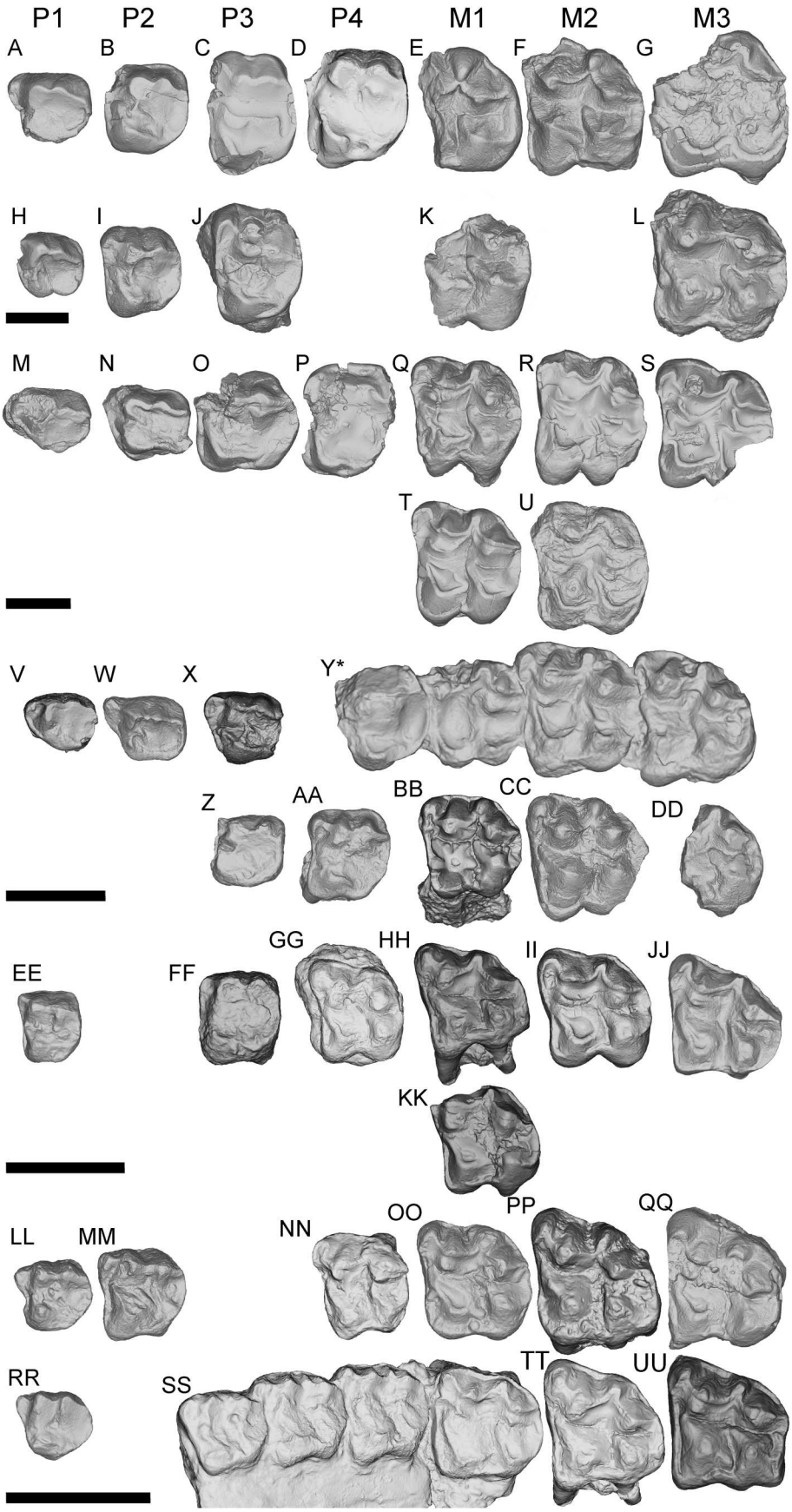

FIGURE 6. Upper teeth of hyracoids from Topernawi in occlusal view. Anterior is to the left. Images are organized by tooth position in columns. Some specimen images have been reversed as indicated to facilitate comparisons between taxa and tooth positions. **A**–**G**, *Nengohyrax josephi*. **A**, KNM-TP 102467, left P1; **B**, KNM-TP 102468 right P2 (reversed); **C**, KNM-TP 102484, left P3; **D**, KNM-TP 102484, left P4, KNM-TP 102475, right P4 (reversed); **E**, KNM-TP 102490, partial left M1; **F**, KNM-TP 102193, left M2; **G**, KNM-TP 102105 left M3; **H**, KNM-TP 102489, left P1; **I**, KNM-TP 102244, left P2; **J**, KNM-TP 102458, right P4 (reversed); **K**, KNM-TP 102156, partial left M1; **L**, KNM-TP 102208, left M3. **M**–**U**, *Abdahyrax philipi*. **M**, KNM-TP 102169, left P1; **N**, KNM-TP 102183, left P2; **O**, KNM-TP 102131, right P3 (reversed); **P**, KNM-TP 102201, right P4 (reversed); **Q**, KNM-TP 102198, left M1; **R**, KNM-TP 102191, right M2 (reversed); **S**, KNM-TP 102486, left M3; **T**, KNM-TP 102247, right M1 (reversed); **U**, KNM-TP 102506, right M2 (reversed). **V**–**DD**, *Geniohyus ewoii*. **V**, KNM-TP 102496, left P1; **W**, KNM-TP 102116, left P2; **X**, KNM-TP 102910, right P3 (reversed); **Y**, KNM-TP 102814, holotype, partial left maxilla with P4–M1; **Z**, KNM-TP 102457, left P2; **AA**, KNM-TP 102097, right P4; **BB**, KNM-TP 102831 (in part), left M1; **CC**, KNM-TP 102101, left M2; **DD**, KNM-TP 102089, partial left M3. **EE**–**KK**, *Thyrohyrax lokutani*. **EE**, KNM-TP 102268, left P1; **FF**, KNM-TP 102969, left P3; **GG**, KNM-TP 102460, left P4; **HH**, KNM-TP 102205, right M1 (reversed); **II**, KNM-TP 102824, left M2; **JJ**, KNM-TP 102479, left M3; **KK**, KNM-TP 102907, right M1 (reversed). **LL**–**UU**, *Thyrohyrax ekaii*. **LL**, KNM-TP 102260, right P1 (reversed); **MM**, KNM-TP 102259, right P2 (reversed); **NN**, KNM-TP 102248, left P4; **OO**, KNM-TP 102254, left M1; **PP**, KNM-TP 102868, left M2; **QQ**, KNM-TP 102223, left M3; **RR**, KNM-TP 102220, left P1; **SS**, KNM-TP 102158, left P2–M1; **TT**, 102205, right M2 (reversed); **UU**, KNM-TP 102734, right M3 (reversed). Scale bars equal 1 cm. Codes at top indicate columns of tooth positions. Asterisk indicates a holotype.

this specimen is a dP4 based on the combination of small size and molar-like features.

Upper Molars—The internal mesial and distal margins of each molar are relatively straight, rather than curved and interlocking (Fig. 6E–G, K, L). The cusps on each crown are moderately convergent, with the buccal cusps placed slightly internal resulting in a well-developed, continuous buccal cingulum. The cingulum crosses the mesostyle transversely. The distal pair of cusps are consistently spaced more closely together than the mesial pair of cusps. Incomplete molars imply the existence of a parastyle, but its morphology is not preserved. The mesostyle is small, approximately half the basal area of the paracone or less. It is located approximately equidistant between the metacone and protocone. The mesostyle is located far buccal to the para- and metacone, but the parastyle and metastyle are closer to being in line with the major cusps, emphasizing the center but not the edges of a "w"-shaped centrocrista. Buccal ribs of enamel are absent on this centrocrista and lingual spurs are absent on the buccal cusps. The metacone has a small, distally oriented postmetacrista.

The cusps on upper molars have relatively small, weakly developed cristae. This proportion is most apparent in the protocone. The protocone has a relatively flat face buccally, and lingually its apex extends only approximately as far as that of the hypocone, not further lingually. The two lingual cusps are of approximately equal size. A continuous cingulum is present around the lingual boundaries of the protocone and is connected to a complete mesial cingulum. The preprotocrista remains independent of the paracone and mesiolabial cingulum. Approximately midway along the preprotocrista, a small cuspule or peak is expressed mesial to the crest. The orientation of the postprotocrista is variable relative to the preprotocrista. On some specimens the two cristae meet at a wide angle at the protocone. In others they are oriented at approximately a 180° angle, forming a continuous crest. Both crests are trenchant and strongly expressed. Buccal spurs of enamel are variably present on the protocone and hypocone. The valley between the protocone and hypocone is relatively straight, oriented toward the mesostyle. A thickening of enamel along a crest extending from either major cusp is frequently present between the protocone and hypocone, potentially identifiable as an entostyle. The hypocone is distolingually expanded, forming a relatively flat lingual wall and a curved, sharp posthypocrista that curves where it joins the posterior border of the tooth. The mesiolingual corner of the hypocone is also expanded, sometimes resulting in a small crest that joins the lingual cingula. The prehypocrista meets the lingual face of the metacone on the mesial side of the cusp. An additional, weakly expressed crest or ridge in the enamel starts on the lingual face of the hypocone and becomes confluent with the lingual cingula around the protocone. Proportionally, the M2 (Fig. 6F) is relatively square in contrast to the M3 (Fig. 6G, L), which is longer than wide. On the M3, the posthypocrista extends to join the postmetacrista forming a distocrista enclosing the talon.

Lower Premolars—Lower premolars lack entoconids as well as any cristids distal to the hypoconid. A partial tooth tentatively interpreted as a p1 (KNM-TP 102150; Fig. 4A) has one large main cusp and a smaller, centrally located secondary cusp without a strong cristid connecting the two. The p3 (KNM-TP 102171; Fig. 4B) has four roots. The paraconid is incorporated into a strongly expressed paracristid. A protoconid and metaconid are closely appressed, with the metaconid slightly smaller and placed distolingually relative to the protoconid. A large hypoconid is connected to the metaconid by a large cristid obliqua. The p4 (KNM-TP 102487, KNM-TP 102162; Fig. 4C, F) has a similar conformation to the p3, but is wider. The protoconid and metaconid are spaced further apart and the paracristid continues down the mesial face of the crown. The cristid obliqua meets

TABLE 1. Measurements (in mm) of fossils of hyracoids from Topernawi. All specimen numbers have the prefix KNM-TP. **Abbreviations**: **L**, length; **W M**, mesial width; **W D**, distal width.

Species	Locus	Specimen	L	W M	W D
Abdahyrax ekuwomi	P1	102169	13.52	10.19	NA
Abdahyrax ekuwomi	P2	102131	16.17	14.98	NA
Abdahyrax ekuwomi	P2	102183	12.45	11.38	NA
Abdahyrax ekuwomi	P2	102185	16.34	13.39	NA
Abdahyrax ekuwomi	P3	102210	15.44	NA	NA
Abdahyrax ekuwomi	P4	102201	14.95	18.5	NA
Abdahyrax ekuwomi	M1	102198	17.73	18.7	NA
Abdahyrax ekuwomi	M1	102247	17.64	19.13	NA
Abdahyrax ekuwomi	M1	102812	15.82	17.94	NA
Abdahyrax ekuwomi	M2	102191	17.9	20.79	NA
Abdahyrax ekuwomi	M2	102506	20.93	18.35	NA
Abdahyrax ekuwomi	M2	102921	19.16	21.48	NA
Abdahyrax ekuwomi	M3	102486	17.5	20.264	NA
Abdahyrax ekuwomi	dp3	102228	13.18	5.2	6.3
Abdahyrax ekuwomi	p1	102936	13.74	7.7	NA
Abdahyrax ekuwomi	p2	102936	13.59	8.54	NA
Abdahyrax ekuwomi	p3	102207	14.2	9.2	10.5
Abdahyrax ekuwomi	p3	102936	14.43	9.95	NA
Abdahyrax ekuwomi	p4	102936	14.27	11.12	NA
Abdahyrax ekuwomi	m2	102214	18.15	13.79	13.52
Abdahyrax ekuwomi	m3	102095	27.15	16.1	14.7
Abdahyrax ekuwomi	m3	102114	28.4	15.44	NA
Geniohyus ewoi	dP4	102831	9.43	9.36	NA
Geniohyus ewoi	P1	102946	7.37	5.85	NA
Geniohyus ewoi	P2	102116	8.12	6.3	NA
Geniohyus ewoi	P3	102498	7.83	7.83	NA
Geniohyus ewoi	P3	102910	7.86	7.33	NA
Geniohyus ewoi	P4	102814	8.44	10.17	NA
Geniohyus ewoi	M1	102512	11.55	10.11	NA
Geniohyus ewoi	M1	102814	10.21	10.67	NA
Geniohyus ewoi	M1	102831	10.22	10.62	NA
Geniohyus ewoi	M2	102101	11.7	12.91	NA
Geniohyus ewoi	M2	102246	11.97	11.31	NA
Geniohyus ewoi	M2	102814	12.26	12.96	NA
Geniohyus ewoi	M2	102814	11.53	13.29	NA
Geniohyus ewoi	M3	102117	13.47	12.7	NA
Geniohyus ewoi	M3	102814	11.73	13.29	NA
Geniohyus ewoi	M3	102814	11.34	13.16	NA
Geniohyus ewoi	p2	102459	8.14	3.9	4.2
Geniohyus ewoi	p3	102186	8.3	4.42	4.93
Geniohyus ewoi	p4	102503	8.37	5.7	5.81
Geniohyus ewoi	p4	102527	9.6	6.7	7.27
Geniohyus ewoi	m1	102104	9.5	7.46	7.4
Geniohyus ewoi	m1	102115	9.26	7.48	7.43
Geniohyus ewoi	m1	102125	9.66	NA	7.14
Geniohyus ewoi	m2	102518	11.3	8.34	8.35
Geniohyus ewoi	m3	102465	14.16	8.4	7.46
Geniohyus ewoi	m3	102815	14.11	8.9	8.13
Nengohyrax josephi	dP4	102177	17	16.64	NA
Nengohyrax josephi	P1	102174	14	11.8	NA
Nengohyrax josephi	P1	102467	12.839	NA	NA
Nengohyrax josephi	P2	102244	12.58	14.63	NA
Nengohyrax josephi	P2	102468	13.32	14.2	NA
Nengohyrax josephi	P2	102481	12.94	13.29	NA
Nengohyrax josephi	P2	102491	13.24	NA	NA
Nengohyrax josephi	P2	102878	13.3	15.55	NA
Nengohyrax josephi	P3	102458	14.13	19.34	NA
Nengohyrax josephi	P3	102484	13.89	19.93	NA
Nengohyrax josephi	P4	102081	14.27	17.92	NA
Nengohyrax josephi	P4	102103	14.3	18.7	NA
Nengohyrax josephi	P4	102721	16.5	17.62	NA
Nengohyrax josephi	M2	102193	22.39	NA	NA
Nengohyrax josephi	M3	102105	21.15	23.81	NA
Nengohyrax josephi	M3	102110	20.62	NA	NA
Nengohyrax josephi	M3	102208	23.75	21.75	NA
Nengohyrax josephi	dp4	102510	15.8	10	10.3
Nengohyrax josephi	p3	102171	14.31	10.58	10.75
Nengohyrax josephi	p3	102779	8.99	3.2	3.56
Nengohyrax josephi	p4	102162	16.7	13.1	12.85
Nengohyrax josephi	p4	102487	17.41	13.96	13.49
Nengohyrax josephi	m1	102086	19.7	14.272	NA

(*Continued*)

TABLE 1. Continued.

Species	Locus	Specimen	L	W M	W D
Nengohyrax josephi	m1	102109	19.56	NA	15.68
Nengohyrax josephi	m2	102113	19.24	NA	NA
Nengohyrax josephi	m2	102172	20.33	17.6	17.4
Nengohyrax josephi	m3	102739	31.75	16.16	16.16
Thyrohyrax ekaii	dP4	102229	6.98	7.42	NA
Thyrohyrax ekaii	P1	102121	4.98	4.48	NA
Thyrohyrax ekaii	P1	102220	4.83	4.47	NA
Thyrohyrax ekaii	P1	102260	5.2	5.5	NA
Thyrohyrax ekaii	P1	102899	4.27	4.17	NA
Thyrohyrax ekaii	P2	102960	4.95	5.31	NA
Thyrohyrax ekaii	P3	102259	8.19	9.2	NA
Thyrohyrax ekaii	P3	102816	5.88	6.2	NA
Thyrohyrax ekaii	P4	102248	8.12	7.17	NA
Thyrohyrax ekaii	M1	102194	7.11	7.67	NA
Thyrohyrax ekaii	M1	102254	7.29	7.83	NA
Thyrohyrax ekaii	M1	102818	6.91	7.51	NA
Thyrohyrax ekaii	M2	102868	7.71	8.62	NA
Thyrohyrax ekaii	M3	102223	7.38	8.9	NA
Thyrohyrax ekaii	M3	102702	6.93	7.74	NA
Thyrohyrax ekaii	M3	102734	8.1	8.4	NA
Thyrohyrax ekaii	p1	102513	4.11	2.32	NA
Thyrohyrax ekaii	p2	102225	5.81	3.51	3.82
Thyrohyrax ekaii	p3	102083	6.73	3.88	4.19
Thyrohyrax ekaii	p3	102180	6.21	4.52	NA
Thyrohyrax ekaii	p3	102226	5.55	3.47	3.85
Thyrohyrax ekaii	p3	102258	5.1	2.58	2.62
Thyrohyrax ekaii	p4	102235	6.45	4.37	4.31
Thyrohyrax ekaii	p4	102250	6.7	4.7	4.67
Thyrohyrax ekaii	p4	102803	6.14	4.29	NA
Thyrohyrax ekaii	m1	102219	7.81	5.15	5.39
Thyrohyrax ekaii	m1	102456	7.79	5.26	5.7
Thyrohyrax ekaii	m1	102708	7.4	4.84	4.43
Thyrohyrax ekaii	m1	102810	7.75	5.3	5.4
Thyrohyrax ekaii	m1	102841	7.24	4.83	4.88
Thyrohyrax ekaii	m2	102173	7.73	5.23	5.13
Thyrohyrax ekaii	m2	102237	7.79	5.47	5.63
Thyrohyrax ekaii	m2	102735	7.86	5.21	5.17
Thyrohyrax ekaii	m2	102766	7.79	5.4	4.98
Thyrohyrax ekaii	m3	102166	10.59	5.32	5.19
Thyrohyrax ekaii	m3	102173	9.52	5.21	4.69
Thyrohyrax ekaii	m3	102204	9.94	5.72	5.55
Thyrohyrax ekaii	m3	102218	10.3	5.33	4.62
Thyrohyrax ekaii	m3	102745	10.43	5.26	5.25
Thyrohyrax ekaii	m3	102786	9.27	4.85	4.6
Thyrohyrax lokutani	dP4	102187	9	8.91	NA
Thyrohyrax lokutani	P1	102268	13.44	14.53	NA
Thyrohyrax lokutani	P3	102969	6.79	81	NA
Thyrohyrax lokutani	P4	102097	8.3	9.14	NA
Thyrohyrax lokutani	P4	102470	7.47	8.72	NA
Thyrohyrax lokutani	M1	102205	9.12	7.83	NA
Thyrohyrax lokutani	M1	102907	7.63	NA	NA
Thyrohyrax lokutani	M2	102824	8.33	9.27	NA
Thyrohyrax lokutani	M3	102479	10.15	10.69	NA
Thyrohyrax lokutani	dp4	102796	8.58	3.91	4.72
Thyrohyrax lokutani	p1	102130	5.77	2.99	3.52
Thyrohyrax lokutani	p1	102158	5.47	3.21	NA
Thyrohyrax lokutani	p2	102263	6.7	3.73	4.5
Thyrohyrax lokutani	p2	102879	6.722	5.193	4.848
Thyrohyrax lokutani	p3	102526	7.56	4.15	4.73
Thyrohyrax lokutani	p3	102526	7.38	4.38	4.84
Thyrohyrax lokutani	p3	102528	6.94	3.72	4.3
Thyrohyrax lokutani	p4	102526	7.69	4.64	4.71
Thyrohyrax lokutani	m1	102464	8.62	5.34	5.41
Thyrohyrax lokutani	m1	102504	8.32	5.49	5.72
Thyrohyrax lokutani	m1	102526	7.97	4.47	4.54
Thyrohyrax lokutani	m1	102075	8.44	4.47	5.9
Thyrohyrax lokutani	m1	102712	8.46	5.27	4.63
Thyrohyrax lokutani	m1	102722	9.2	NA	5.92
Thyrohyrax lokutani	m1	102782	9.94	5.92	5.3
Thyrohyrax lokutani	m2	102142	8.95	6.4	6.35
Thyrohyrax lokutani	m3	102463	12.49	5.77	5.28
Thyrohyrax lokutani	m3	102526	11.2	5.17	5.17

the protoconid at the postvallid. One tooth has the same conformation of cusps and crests but is much narrower than long (KNM-TP 102510; Fig. 4B): it is identified as a dp4.

Lower Molars—An increase in crown area along the lower molar row is strong: the m2 is ~1.3 times the area of the m1, and the m3 ~1.8 times the area of the m1 (Figs. 4D–E, 7). The talonid of m1–2 is slightly longer than the trigonid. The crown base is inflated buccally and lingually, though the walls of the cusps themselves are subvertical. Lower molars lack mesoconids and spurs of enamel. Both main cusp pairs on the trigonid (protoconid and metaconid) and talonid (hypoconid and entoconid) are transversely oriented, the line connecting each pair being approximately perpendicular to the long axis of the tooth (Fig. 4D, E, G).

The trigonid basin is enclosed by a combination of the paracristid and premetacristid. The paracristid is continuous and curves gently, rather than sharply, around the trigonid. It lacks a cuspidate paraconid. The metaconid is slightly distally offset from the protoconid and elevated above the protoconid. The postmetacristid is small such that it does not extend much past the postvallid. A buccal cingulid is present, strongly expressed around the hypoflexid but discontinuous around the hypoconid.

The cristid obliqua ascends the postvallid, terminating between the metaconid and protoconid. The entoconid and hypoconid are distinct cusps with a small cristid that is lost early as the tooth wears. The cristid obliqua and the small hypocristid both meet at the hypoconid, but the junction is gently rounded rather than "v"-shaped. The hypoconid is slightly larger than the entoconid. It is also mesiobuccally inflated, and accordingly more rounded than triangular in its footprint on the crown. The mesiobuccal face of the entoconid is flat or expanded, limiting the size of the talonid basin. The entocristid is weakly expressed relative to the size of the entoconid even though the entocristid and postmetacristid together nearly enclose the talonid basin. A small peak in the postcingulid is all that remains of a hypoconulid on the m1 and m2, but it is connected to the hypoconid by a narrow cristid.

Type Locality—Hill 2, Topernawi, Ekitale Basin, west of Lake Turkana, Kenya; stratigraphic unit U4, Topernawi Fm., mid-Oligocene.

Remarks and Comparisons—*Nengohyrax josephi* differs from other taxa assigned to Geniohyidae by features beyond those listed in the diagnosis. It differs from established species of *Bunohyrax*, such as *Bunohyrax fajumensis*, in having a more fully enclosed trigonid basin and a stronger postmetacristid on the lower molars. The connection between the entoconid and hypoconid is also stronger, and the basins themselves lack spurs of enamel. On the upper molars, the two taxa share similarities in the relative size and placement of the mesostyle, but differ in molar dimensions and in the reduction of central spurs of enamel on the major cusps.

It differs from the unnamed species of *Bunohyrax* from Chilga in having a less distinct, shorter, non-recurved paracristid; a reduced preentocristid; weaker postmetacristid; and absence of spurs on major cusps of the lower molars. It also has more equal-length trigonid and talonid, in contrast to the species from Chilga which has a relatively shorter trigonid, resulting in shorter and wider lower molars in *N. philipi* (Rasmussen & Gutierrez, 2010).

Nengohyrax differs from *Geniohyus* in being distinctly larger in size, in addition to multiple features of upper and lower teeth. On the lower molars of *Nengohyrax,* the m2 entoconid is also distinctly smaller than the hypoconid in constrast to the more equally sized cusps on the m2 of *Geniohyus.* On the upper molars of *Geniohyus*, the prehypocristae on the upper

M1–2 are oriented mesial to the mesial wall, versus meeting the mesial wall of the metacone in *Nengohyrax*. The M2 mesostyle is small, less than half the area of the protocone in *Geniohyus*, but relatively larger in *Nengohyrax*. Finally, the M2 and M3 are similarly sized in *Geniohyus*, whereas the M3 is larger in *Nengohyrax*.

Nengohyrax differs from *Pachyhyrax* in having less molarized premolars and lacking pre- and posthypocristids on the m1, as well as in having entoconids on the p3 and p4. *Nengohyrax* lacks the continuous buccal cingulum and relatively strong postmetacristid that are seen on lower molars of *Pachyhyrax*. Like *Geniohyus*, *Pachyhyrax* differs from *Nengohyrax* in lacking a strong premetacristid that encloses the trigonid. The entoconid is more posteriorly placed in *Pachyhyrax*. On upper teeth, *Nengohyrax* lacks the more molarized features of the premolars, specifically the P2, P3, and P4 hypocone and P4 entocristia. It also lacks lingual spurs on M1–2 buccal cusps, and interlocking mesial and distal walls of the upper molars. The prehypocristae on the M1–2 of *Pachyhyrax* are oriented mesial to the mesial wall of the metacone, unlike those of *Nengohyrax* that meet the mesial wall. The M2 mesostyle of *Pachyhyrax* is small and closer to the metacone than paracone, but that of *Nengohyrax* is large and more equidistant between the two cusps.

Nengohyrax differs from *Brachyhyrax* in all of the ways in which it differs from *Abdahyrax philipi*: *Nengohyrax* has more strongly expressed buccal cingula on the lower molars, more rounded entoconids that expand further into the talonid basin, and smaller postmetacristids. On the upper molars *Nengohyrax* has a relatively more crestiform appearance, a smaller mesostyle, lacks the weak mesially directed crest on the lingual face of the hypocone that is distinctive in *Abdahyrax philipi*, and has a more buccally placed protocone. On the upper posterior premolars, *Brachyhyrax* has hypocones that are lacking in *A. josephi*.

Compared with the unnamed species of pachyhyracine from Losodok and Nakwai, *N. philipi* has more robust and wider upper molars with cusps arranged in a more rectangular shape, as well as a less buccally directed postprotocrista on the upper molars. No definitive lower molars have yet been figured, but the lower premolars of the Nakwai pachyhyracine are more elongate with well-developed entoconids connected to hypoconids by strong crests, both of which are completely lacking in the premolars of *N. philipi*.

ABDAHYRAX PHILIPI gen et. sp. nov.
(Figs. 4, 5, and 6; Table 1)

Holotype—KNM-TP 102936, left dentary with p1–m3 (Fig. 4H).

Etymology— Genus named for Abdullah Ekuwom, who prepared some of the first specimens of the genus; species named for Philip Ekadeli, who found some of the first specimens of this species.

Referred Specimens—KNM-TP 102078 right m3, KNM-TP 102095 right m3, KNM-TP 102114 left m3, KNM-TP 102123 upper molar, KNM-TP 102131 right P3, KNM-TP 102141 left upper premolar, KNM-TP 102169 left P1, KNM-TP 102183 left P2, KNM-TP 102185 left P2, KNM-TP 102191 right M2, KNM-TP 102198 left M1, KNM-TP 102201 right P4, KNM-TP 102207 right p3, KNM-TP 102210 right P3, KNM-TP 102214 left m2, KNM-TP 102228 left dp3, KNM-TP 102231 right upper molar, KNM-TP 102232 left dP4, KNM-TP 102238 right upper molar, KNM-TP 102247 right M1, KNM-TP 102249 left m3, KNM-TP 102266 right upper molar, KNM-TP 102272 right ?p4, KNM-TP 102486 left M3, KNM-TP 102506 right M2, KNM-TP 102509 left P1, KNM-TP 102511 left m3.

Diagnosis—Apomorphies within Geniohyidae: p4 hypoconid reduced, less than half height of protoconid; metaconid distal to protoconid; lower molar buccal cingulids absent; cristid obliqua-hypoconid junction meets at sharp angle; recurved paracristid; hypoconid triangular; P4 protocone shifted mesial to paracone; labial bulge of protocone on M1–2; M2 approximately equal in size to M1; M2 mesostyle large; molar mesostyles closer to metacone than protocone; similar distance between distal and mesial cusp pairs on M1. Differs from other non-*Brachyhyrax* geniohyids: presence of reduced parastyle; weak metastyle on upper molars; strong and relatively continuous pre- and postprotocristae and pre- and posthypocristae; strongly expressed mesiolingual cingulum; frequent appearance of entostyle or additional small crests of enamel in that region of crown; protocone with distobuccally oriented expansion, called a mesoprotocrista by Pickford (2004); trigonid proportionally short compared with talonid; notch separating entoconid and hypoconid; strong entocristid. Differs from *Brachyhyrax*: lingual space between upper molar protocone and hypocone more deeply emarginated; completely enclosed m3 trigonid; presence of weakly expressed hypocone on upper premolars, absence of mesostyle on upper premolars.

Description

Upper Premolars—On the premolars, a hypocone is present but weakly expressed. On worn teeth, it can only be recognized through an expansion of worn enamel on the distolingual margin of the crown. Cusps are internalized, and there is a broad, nearly continuous cingulum around the entire crown. This cingulum is expanded in the region of the parastyle, though it is not clear whether a distinct parastyle itself is present. Each premolar has a large protocone. A paracone and metacone are also present but smaller and closely appressed to each other. The paracone and protocone are located at approximately the same point along the mesiodistal axis of the tooth. Mesostyles and centrocristae are absent. Compared with other premolars in the tooth row, the P1 (KNM-TP 102169; Fig. 6M) and P2 (KNM-TP 102183; Fig. 6N) is smallest and most anteroposteriorly elongate relative to its buccolingual width. The P3 (KNM-TP 102131. Fig. 6O) is similarly longer than wide, but not to as great an extent. The P4 (KNM-TP 102201; Fig. 6P) is wider than long. The P4 is the only locus with preserved bases of roots, indicating that it has four or more.

Upper Molars—The increase in crown area along the upper molar row is slight: the M2 is only ~1.2 times the area of the M1, and the M3 only ~1.1 times the area of the m1 (Fig. 7).

Upper teeth and lower teeth are generally brachydont (Fig. 6Q–U). The mesial margin of each molar is concave, interlocking with distal margins of preceding teeth. Buccal and lingual cusps are moderately convergent and slightly internalized, leaving distinct cingula around the crown, including a well-defined mesial cingulum. The buccal cingulum is continuous. It traverses the mesostyle without ascending. The distobuccal margin of the tooth around the metacone is convex. Cusps lack lingual or buccal spurs of enamel.

The parastyle is small, slightly over half the area of the paracone. It is situated mesial to the paracone and is not strongly hook-like in structure. Each of the buccal cusps are rounded and inflated, resulting in the presence of buccal folds between parastyle, paracone, mesostyle, and metacone. The mesostyle is large, greater than half the basal area of the paracone, and is located closer to the metacone than it is to the paracone. The metastyle is small and distally oriented.

The lingual cusps have flattened buccal faces bounded by cristae. A strong mesiolingual cingulum is present around the protocone. The protocone is pinched, much longer along a mesiolingual-distobuccal axis than a mesiobuccal-distolingual axis. This shape results in a mesiolingual extension of the cusp beyond the preprotocristae as well as a distobuccally oriented

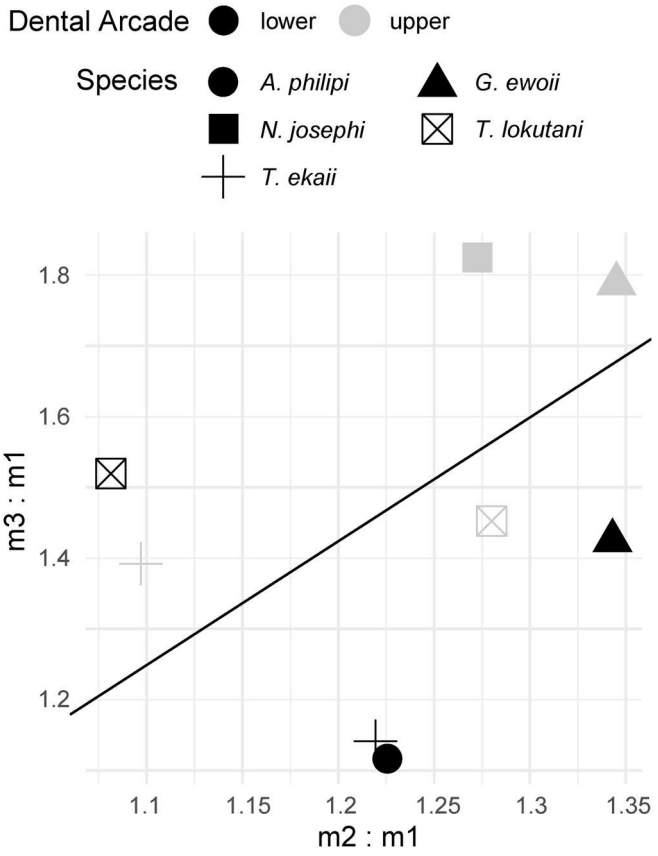

FIGURE 7. Proportions of molar crown area for each species of hyracoid found at Topernawi. X-axis shows second molar area relative to first molar area. Y-axis shows third molar area relative to first molar area. Upper molar proportions are in triangles, lower molar proportions are in circles. Some species are missing upper or lower proportions because of lack of specimens representing certain loci. The line through the graph shows the molar proportions predicted by the inhibitory cascade model for lower teeth, where $1 + (m3/m1) = 2(m2/m1)$.

expansion that is distinct, but less trenchant and sharp than a spur of enamel. The pre- and postprotocrista are large and well-developed, giving the structure a more crestiform appearance. A small expansion of enamel along the preprotocrista is interpreted as a paraconule, best visible on the M3 (KNM-TP 102468; Fig. 6S). The preprotocrista itself remains distinct, confluent with neither the mesiolabial cingulum nor the parastyle. The well-developed preprotocrista-postprotocrista pair and prehypocrista-posthypocrista pair each meet at their respective protocone and hypocone, forming a wide-angled "v" shape.

The lingual margin between the protocone and hypocone is moderately emarginated. An entostyle is frequently present along the lingual crown margin at this emargination. The hypocone and protocone are similar in size. The prehypocrista is oriented toward the paracone, ending mesial to the mesial wall of the metacone. The posthypocrista is present and sharp.

On the M1 (Fig. 6Q, T), the distance between the distal cusp pairs (hypocone and metacone) is approximately equal to the distance between the mesial cusp pairs (protocone and paracone). The M2 (Fig. 6R, U) is notably wider than long. The M2 and M3 are similar in size.

Lower Premolars—A single lower premolar is tentatively identified as a p3 (KNM-TP 102207; Fig. 4I). It has at least three roots. On the worn crown surface there is evidence for a mesially oriented paracristid. It is connected to either a protoconid or a closely appressed protoconid-metaconid pair. A centrally located cristid obliqua is present in addition to lingual and buccal cristids extending distally from the main cusp on the trigonid. The cristid obliqua ends on the distal margin of the tooth in a centrally placed hypoconid. A tooth of much narrower width, but with a similar length and with a similar arrangement of cusps, is tentatively identified as a dp2 (KNM-TP 102228; Fig. 5C).

On the hemi-mandible with associated premolars (KNM-TP 102936; Fig. 4H), the p1 has a large, midline protoconid cusp bearing a distally oriented central crest ending in a much smaller, midline cuspid identified as the hypoconid. The crest branches into an additional distobuccal fork and a weaker distolingual fork. The p2 has a similar suite of features, plus a small but distinct paraconid connected to the protoconid by a crest. On the p3, the paraconid is relatively more strongly developed, the hypoconid is located more buccally compared with the p2. Either a small metaconid is present closely appressed to the protoconid, or the protoconid is wide with two distinct crests on the buccodistal and linguodistal corners.

The p4 bears a distinct metaconid placed slightly further distally than the protoconid. The paracristid remains mesial to the protoconid. Like other premolars, the protoconid retains a distinct distobuccal crest. The hypoconid is buccally placed, connected by the cristid obliqua to the postvallid at the notch between the protoconid and metaconid. Entoconids are absent on all premolars.

Lower Molars—The lower molar trigonids and talonids are about equal in height. The trigonid is relatively short in comparison to the length of the talonid. The lingual and buccal walls of the cusps are basally inflated, with the hypoconid and protoconid still placed relatively peripherally on the crown surface. Spurs of enamel protrude from the protoconid and metaconid into the trigonid basin. The trigonid is fully enclosed, anteriorly by the paracristid and premetacristid and posteriorly by the protoconid and metaconid, although the cristid between the latter cusp pair is incomplete. The paraconid is placed slightly lingual relative to the protoconid. The protocristid is low and narrow, approximately perpendicular to the long axis of the tooth. The metaconid is higher than the protoconid. The presence of both a strong premetacristid and strong postmetacristid gives the metaconid an appearance of a small cusp traversed by a single, strong, continuous cristid. The strong postmetacristid nearly meets an equally strong entocristid to enclose the talonid basin.

Buccal cingulids are absent, although an anterobuccal cingulid is present. The cristid obliqua connects to the postvallid between the protoconid and metaconid. It meets the hypocristid on the hypoconid at a sharp angle. The entoconid and hypoconid are similar in size. They are approximately as strongly connected to each other as the hypoconid is to the cingular peak on the distal face of the molar, resulting in a notch, or flexid, around the distobuccal face of the entoconid. The mesiobuccal face of the entoconid is concave, contributing to the appearance of an expansive talonid basin. Both cristids are low and poorly developed. The entoconid and hypoconid form a line that is approximately perpendicular to the long axis of the tooth. The hypoconid is relatively small and uninflated relative to the size of the connecting cristids, resulting in a relatively triangular shape to the cusp in occlusal view. The postcingulid is peaked centrally where a hypoconulid might be. The m2 entoconid is similar in size to the hypoconid.

On the m3, the trigonid is completely enclosed by a combination of the paracristid and premetacristid. Strong buccal, anterior cingulids are present. The hypoconulid lobe on the m3 is wide, more than half the width of the talonid, and is

surrounded by a continuous, low crest. A single, large cusp is present on the distobuccal corner of the lobe.

Type Locality—Blue Hill, Topernawi, Ekitale Basin, west of Lake Turkana, Kenya; stratigraphic unit U4, Topernawi Fm., mid-Oligocene.

Remarks and Comparisons—An analytically based assignment of *A. philipi* to *Brachyhyrax* is not yet possible because other species of *Brachyhyrax* have not yet been included in phylogenetic character-taxon matrices. The addition of these taxa from other sites is beyond the scope of this current study. However, similarities are intriguing and should be investigated further.

Abdahyrax shares with other species of *Brachyhyrax* the presence of a reduced parastyle; a weak metastyle; strong and relatively continuous pre- and postprotocristae and pre- and posthypocristae; a mesostyle located closer to the metacone than the paracone, a strongly expressed mesiolingual cingulum; the frequent appearance of a pericone or additional small crests of enamel in that region of the crown; a protocone with a distobuccally oriented expansion (=mesoprotocrista); a notch separating the entoconid and hypoconid; a trigonid notably anteroposteriorly shorter than the talonid; and a strong entocristid. *Abdahyrax* differs from *Brachyhyrax* in having a more deeply emarginated lingual space between the protocone and hypocone; a completely enclosed m3 trigonid, and in having premolars that are less molarized in terms of a very weak hypocone being present.

Abdahyrax differs from *Bunohyrax* in having less molarized premolars, specifically lacking a p2 metaconid and p2–p4 entoconid, as well as having a relatively smaller p2 and p3 hypoconid and less strongly expressed p4 protolophid. The metaconid is more distally placed on the p4 and the p4 talonid is wider in *Abdahyrax*. Lower molars of *Abdahyrax* differ in having a sharp junction of the cristid obliqua, a relatively larger premetacristid, and an uninflated, triangular hypoconid. Upper molars differ in having a more mesially shifted protocone, a parastyle situated mesially, and a proportionally smaller M3.

Abdahyrax differs from *Geniohyus* in having a relatively smaller p2 hypoconid and metaconid. *Geniohyus* has a more rounded cristid obliqua junction and a mesially open trigonid basin without a recurved paracristid. In *Geniohyus*, the entoconid is comparatively much smaller than the hypoconid, and the hypoconid itself is inflated and rounded. *Abdahyrax* lacks a hypocone on the P3. On upper molars, *Abdahyrax* differs from *Geniohyus* in having a mesially shifted protocone and parastyle, interlocking mesial and distal walls of molars, and a relatively large M2 mesostyle located closer to the metacone than paracone.

Abdahyrax differs from *Pachyhyrax* in having less molarized premolars, specifically a less strongly expressed p2 hypoconid, metaconid, and entoconid; p3 hypoconid, entoconid, and metastylid; and p4 entoconid. Unlike *Pachyhyrax*, *Abdahyrax* lacks a lower molar buccal cingulum. It has a sharp cristid obliqua junction, an enclosed lower molar trigonid, and an uninflated, triangular hypoconid. On upper molars, *Abdahyrax* differs in having a mesially shifted protocone, a mesially shifted parastyle, and a relatively larger M2 mesostyle.

GENIOHYUS EWOII sp. nov.
(Figs. 4, 5, and 6; Table 1)

Holotype— KNM-TP 102814, left partial maxilla P4–M3, and right partial maxilla, M2–M3, associated (Fig. 6Y, S5A–B).

Etymology—Named for Francis Ewoi, who discovered the type specimen.

Referred Specimens—KNM-TP 102089 left M3, KNM-TP 102097, right P4, KNM-TP 102101 left M2, KNM-TP 102104 left m1, KNM-TP 102115 right m1, KNM-TP 102116 left P2, KNM-TP 102117 left M3, KNM-TP 102120 right M3, KNM-TP 102125 left m1, KNM-TP 102157 right dP4, KNM-TP 102164 right lower molar, KNM-TP 102186 left p3, KNM-TP102187, left dP4, KNM-TP 102202, left dP3, KNM-TP 102246 left M2, KNM-TP 102253 left m2, KNM-TP 102457 left P3, KNM-TP 102459 right p2, KNM-TP 102465 right m3, KNM-TP 102498, left P3, KNM-TP 102502 right lower molar, KNM-TP 102503 right p4, KNM-TP 102512 left M1, KNM-TP 102518 right m2, KNM-TP 102527 right p4, KNM-TP 102814, left partial maxilla with P3–M3, right partial maxilla with M2–M3, KNM-TP 102831, left partial maxilla with dP4–M1, KNM-TP 102910, right P3, KNM-TP 102946, left P1.

Diagnosis—Apomorphies within Geniohyidae: P2 protocone small; m3 hypoconid reduced, unicuspid. Differs from other geniohyids: reduction in relative size of premolar hypoconids concurrent with widened premolar talonid basins with small but distinctly present entoconids; absence of spurs in trigonid basins and upper molar buccal cusps; protocone with labial extension; interlocking molar walls.

Description

Upper Premolars—Teeth are generally brachydont. Premolars lack mesostyles, but have small parastyles. The P1 and P2 (KNM-TP 102496, KNM-TP 102116; Fig. 6V, W) have a metacone that is closely appressed to the paracone. More distal premolars have a larger, more distinct metacone. All premolars have a parastyle and a large and well-developed protocone. The hypocone is absent. The P3 has at least four roots (Fig. 6X, Z). A P4 is preserved in a partial maxilla along with all three left upper molars (KNM-TP 102814; Fig. 6Y, AA). Parts of at least four roots are exposed above the alveolar face of the maxilla. The paracone and metacone each bear a weak ridge on the lingual face. A straight, distally directed postmetacrista extends from the cusps. The protocone and paracone are arranged in a line approximately perpendicular to the long axis of the tooth row.

Some specimens appear superficially similar to upper molars but are notably smaller, with four approximately equally sized cusps, a relatively small parastyle, a prominent mesostyle, and an entostyle, similar to the molars of this taxon. We identify these teeth as deciduous premolars (dP3, dP4; KNM-TP 102202, KNM-TP 102157, KNM-TP 102187, anterior tooth of KNM-TP 102831; Fig. 5D–G).

Upper Molars—Increase in crown area along the upper molar row is moderate: the M2 is ~1.3 times the area of the M1, and the M3 ~1.4 times the area of the M1 (Figs. 6Y, BB–DD, 7). The molars have mesial and distal walls that interlock between adjacent teeth, with distinctly concave mesial margins. The cusps are large and rounded relative to the size of connecting crests. Their size and shape results in buccal folds between the cusps and smaller structures such as the parastyle and mesostyle. The four main cusps, the protocone, paracone, metacone, and hypocone, are similar in size. Metaconules are absent.

The buccal cusps and structures are placed far on the periphery of the crown, such that the cingula present are small and discontinuous, and there is little space between the metacone and the very small metastyle, which is distally oriented. The parastyle is relatively small compared with the size of the paracone, and is weakly buccally oriented. No ribs are present on the centrocrista. The mesostyle is approximately one-third to one-half the basal area of the paracone. It is located approximately equidistant between the paracone and metacone. The buccal cingulum is continuous, and crosses the mesostyle transversely. The buccodistal margin around the metacone between the mesostyle and metastyle is relatively straight.

The protocone bulges labially. A thickening on the preprotocrista is interpreted as a small, weakly expressed paraconule (Court & Hartenberger, 1992). The preprotocrista itself remains distinct from the parastyle and mesiolabial cingulum throughout its length. The postprotocrista is equally well expressed as the preprotocrista and is variably oriented distally or buccodistally. The lingual cingulum is continuous around the protocone and connects a complete mesial cingulum to the postcingulum. A small entostyle is present on the lingual cingulum between the protocone and hypocone on some specimens. The valley between the protocone and hypocone is crescent-shaped and oriented toward the distal face of the paracone. The prehypocrista is oriented toward the mesostyle, mesial to the mesial wall of the metacone. The posthypocrista is distinct and oriented distally.

The distance between the distal cusp pair on the M1 (KNM-TP 102512; Fig. 6Y, BB) is shorter than the distance between the mesial cusp pair. A distobuccally oriented spur of enamel is present on the hypocone, and is particularly strongly expressed on the M3. An additional lingual spur, or small crest of enamel, variably extends distolingually from the metacone or metastyle of the M3 (KNM-TP 102814; Fig. 6Y, DD). The posterior cingulum is variable in the presence of cuspules or bumps, especially on the M3. The posthypocrista extends around the distal margin of the tooth to form a low distocrista.

Lower Premolars—One of the isolated lower premolars in the hypodigm could be either a p1 or a p2 (KNM-TP 102459; Fig. 4L), while another could be a p2 or a p3 (KNM-TP 102186, Fig. 4M). The first is provisionally identified as a p1 based on its similarity in size to KNM-TP 102186, which is provisionally identified as a p2 based on the gap in size between it and a p4, KNM-TP 102527 (Fig. 4N). However, the p1 may be a dp1 if the root pattern is similar to that of the extant *Procavia capensis* (McKay et al., 2022). The p1 has two roots. The crown has a large main cusp, identified as the protoconid, a smaller anterior cusp identified as the paraconid, and a single cusp on the talonid identified as the hypoconid. The protoconid has prominent buccal and posterolingual ridges, as well as a cristid obliqua extending up the distal wall of the protoconid. The p2 (KNM-TP 102186) has four roots. The trigonid has a closely appressed protoconid and metaconid, and a mesially oriented paracristid. The talonid has a hypoconid connected to the metaconid by a strong cristid obliqua. Distal expansions on both the protoconid and metaconid give the impression that there are furrows on either side of the cristid obliqua. The hypoconid is located slightly lingual to the central axis of the tooth.

The p4 (KNM-TP 102527; Fig. 4N) talonid is wider than the trigonid. The trigonid contains three cusps, a small paraconid and larger, similarly sized protoconid and metaconid. The two cusps are arranged in a transverse line approximately perpendicular to the long axis of the tooth. The paracristid on the p4 is straight and mesially oriented. On the trigonid, both a hypoconid and entoconid are present and similar in size. The hypoconid is more buccally placed, closer to the periphery of the crown, than it is on preceding premolars. The cristid obliqua is relatively small and connects to the postvallid between the protoconid and metaconid. An incipient protocristid connects the two cusps. No lower deciduous premolars have yet been recognized.

Lower Molars—Increase in crown area along the lower molar row is substantial: the m2 is ~1.3 times the area of the m1, and the m3 ~1.8 times the area of the m1 (Figs. 4O–Q, 7). Molar cusps are conical, round, with very weakly developed crests, making cusps appear to be more clearly discrete structures. The conical form of the cusps leads the bases to expand into the trigonid and talonid basins. The buccal and lingual molar walls are subvertical, with most cusps located on the periphery of the crown base. The protoconids of anterior molars are more centralized. The mesiobuccal cingulid is distinct. The trigonid and talonid are similar in height. Both the mesial and distal cusp pairs are oriented approximately perpendicular to the long axis of the tooth. Mesoconids and spurs on the trigonid basin are absent.

The paracristid is short and weakly expressed, much lower and less sharp than other cristids or cusps on the tooth. It appears as a relatively straight mesiolingual extension from the protoconid. The protocristid is weak, resulting in the appearance of variably present indentations in the crest where the two molars are closely spaced from one another but not connected (KNM-TP 102104; Fig. 4O). The metaconid is elevated above the protoconid. The metaconid and entoconid are similar in height. A postmetacristid is present, though much smaller than the area of the metacristid.

Internal spurs or large crenulations of enamel are present within the talonid basin. The cristid obliqua ascends the postvallid either on the protoconid or between the metaconid and protoconid. The hypocristid is present but low and thin relative to the cusps it connects. It connects the cusps relatively mesially, resulting in the appearance of a distal indentation or flexid around the entoconid. The hypocristid and cristid obliqua both connect to a relatively large hypoconid, but do not meet; there is no distinct "v" shape where the two cristids meet. An entocristid expands mesially from the entoconid for greater than half the length of the pre-entoconid talonid basin, although the basin remains open. A crest connects the hypoconid and hypoconulid, even when the hypoconulid is a small peak on the distal cingulum of the tooth in more anterior molars.

The m1 talonid is longer than the trigonid. A strong buccal cingulid is present on the m2. The m2 entoconid is much smaller than the hypoconid. In contrast to the m1, the protoconid and hypoconid are much larger than their lingual cusp pairs, the metaconid and entoconid, on the m2 and m3. This relative size, as well as a relatively short talonid, results in a short cristid obliqua. The entocristid is weakly expressed on the m3 (KNM-TP 102456, Fig. 4Q) such that the small talonid basin is lingually open. On the hypoconulid lobe there is a single, strong central crest connecting the hypoconid and a similarly sized hypoconulid, forming a buccal border to the lobe. The hypoconulid is the sole cusp on the structure. The presence of the central crest results in a deep flexid between the hypoconid and hypoconulid. The rest of the crown surface of this lobe is open, including a small indentation or flexid between the hypoconid and entoconid.

Type Locality—Hill 4, Topernawi, Ekitale Basin, west of Lake Turkana, Kenya; stratigraphic unit U4, Topernawi Fm., mid-Oligocene.

Remarks and Comparison—The holotype consists of two fragments of maxilla that do not physically articulate, leaving open the question of whether they are associated elements from the same individual. We work under the hypothesis that these elements are associated for the following reasons. First, the specimens were found within centimeters of each other in the field. Second, the bone of both specimens is a similar tan color and the enamel is a similar pattern of white with blue and brown regions, consistent with similar preservation history. Third, the assembled teeth contain non-overlapping elements (e.g., no duplicate right M2s). Fourth, antimeres are nearly identical in size and wear stages, in addition to having similar overall morphology.

Geniohyus ewoii is similar to other species of *Geniohyus* in its relatively small mesostyle and parastyle, as well as its conical lower molar cusps, relatively small entoconid, and strong cristid connecting the hypoconid to the hypoconulid. In the last character it is also similar to the lower molars of *Bunohyrax* sp. from Chilga (Rasmussen & Gutierrez, 2010). However, *Geniohyus ewoii* differs from other species of *Geniohyus* in the presence of more elongate anterior premolars, a more molarized p4 with

entoconid and incipient hypolophid, absence of a distinct hypoconulid, and relatively larger upper molar cusps compared with upper molar cristae. It further differs from *Geniohyus dartevellei* from Malembo (Angola) in the absence of a distal wall on the hypoconulid loop, and the presence of a stronger paracristid forming a more distinct trigonid basin on the m3. Its entoconid is smaller than those of *Bunohyrax* sp. from Chilga, and overall the teeth are more brachydont than those described for the unnamed pachyhyracine from Losodok and Nakwai (Rasmussen & Gutierrez, 2009). Further work will be necessary to more clearly differentiate *Geniohyus ewoii* from unnamed eastern African material, including specimens from Chilga and the pachyhyracine from Losodok/Nakwai (Kappelman et al., 2003; Rasmussen & Gutierrez, 2009).

Geniohyus ewoii differs from *Bunohyrax* and *Nengohyrax* in its smaller size, and in the following details. On the lower premolars, *Geniohyus ewoii* has a p1 paraconid and a relatively wider p4 talonid. On the lower molars, *Geniohyus ewoii* has a straight paracristid (in contrast to a recurved paracristid); an entoconid smaller than the hypoconid (in contrast to a large entoconid); subvertical lingual molar walls with a peripherally placed entoconid and metaconid (in contrast to more centrally placed cusps); and a reduced, unicuspid m3 hypoconulid (in contrast to a more strongly developed hypoconulid). On upper premolars, *Geniohyus* has a poorly differentiated P2 metacone and small P2 protocone. On the upper molars it has interlocking mesial and distal upper molar margins and a labial bulge on the protocone. In contrast, these features are absent or reduced in *Bunohyrax* and *Nengohyrax* with few exceptions.

Geniohyus ewoii differs from *Brachyhyrax* and *Abdahyrax* in smaller size as well as more molarized premolars, specifically in terms of having a p1 paraconid, p2 metaconid, well-developed p4 entoconid, and an incipient p4 hypolophid. On the lower molars, *Geniohyus ewoii* has a straight (unrecurved) paracristid; a more rounded, inflated hypoconid with a proportionally smaller entoconid; subvertical lingual molar walls with a peripherally placed entoconid and metaconid; and a reduced, unicuspid m3 hypoconulid. Its upper premolars are less molarized, specifically in terms of lacking a P3 and P4 hypocone and in having a poorly differentiated P2 metacone and small P2 protocone. Upper molars of *Geniohyus ewoii* have a proportionally smaller M2 mesostyle equidistant between the paracone and metacone, a proportionally shorter distance between the M1 distal cusp pair than the mesial cusp pair, a M3 proportionally larger than M2, and a buccally oriented M1–2 parastyle.

Geniohyus ewoii differs from *Pachyhyrax* in its smaller size; in lacking a p4 entoconid and entocristid; in having a reduced, unicuspid m3 hypoconulid; in having a gently rounded cristid obliqua-hypocristid junction (as opposed to a sharp angled junction); in having an entoconid much smaller than the hypoconid and in the chord between the two perpendicular to the long axis of the tooth (in contrast to a larger, distally shifted entoconid in *Pachyhyrax*); and in having subvertical lingual molar walls with a peripherally placed entoconid and metaconid. *Geniohyus* has less molarized premolars, particularly in terms of lacking a P3 and P4 hypocone, and having a poorly differentiated P2 metacone with a small P2 protocone. The M2 mesostyle is equidistant between the paracone and metacone, and the protocone and paracone form approximately a right angle to the buccal face of upper molars, in contrast to the mesostyle and protocone placement in *Pachyhyrax*.

HYRACOIDEA INCERTAE SEDIS
THYROHYRAX Meyer, 1973
THYROHYRAX LOKUTANI sp. nov.
(Figs. 4, 5, and 6; Table 1)

Holotype—KNM-TP 102526 right canine or upper incisor, p3, p4, left p2 trigonid, p3, m1, m3 (Figs. 4U, Z, BB, S5C–L).

Etymology— Named for Joseph Lokutan, who discovered multiple important specimens of this species.

Referred Specimens—KNM-TP 102075 right m1, KNM-TP 102091 left upper premolar, KNM-TP 102130 left p2, KNM-TP 102142 right m2, KNM-TP 102147 left dP3, KNM-TP 102149 left upper deciduous premolar, KNM-TP 102158 right p1, KNM-TP 102187 left dP4, KNM-TP 102205, right M1, KNM-TP 102222 right lower molar, KNM-TP 102263 right p2, KNM-TP 102268, left P1, KNM-TP 102463 left m3, KNM-TP 102464 left m1, KNM-TP 102470 left P4, KNM-TP 102479 left M3, KNM-TP 102501 left dP4, KNM-TP 102504 right m1, KNM-TP 102528 left p3, KNM-TP 102824, left M2, KNM-TP 102907, right M1, KNM-TP 102969, left P3,

Diagnosis— Diagnosed as *Thyrohyrax* based on apomorphies: small size, molarized premolars with distinct entoconids, selenolophodont cheek teeth with zig-zag lophs. Apomorphy within *Thyrohyrax*: large P4 mesostyle. Differs from *Thyrohyrax kenyaensis* in: less frequent incidence of entostyle; valley between protocone and hypocone oriented away from mesial margin of tooth; more strongly recurved p4 paracristid; enclosed trigonid basin on m2 and m3. Differs from *Thyrohyrax ekaii* and *T. microdon*: relatively larger p4 in comparison to m1; metaconid distal to protoconid; entoconid distal to hypoconid; proportionally longer molars; relatively larger upper molar distal cusps; more strongly expressed lophs between buccal crown features; valley between protocone and hypocone offset distally from mesostyle; M1 distal cusp pairs closer to each other than mesial cusp pairs; less continuous labial cingulum around base of M2 protocone; more labial extension of protocone; relatively larger M2 than M1; mesostyle equidistant between protocone and metacone.

Description

Upper Premolars—P2s of this taxon have not yet been identified among the fossils from Topernawi. Teeth are relatively brachydont. P1 (Fig. 6EE) and P3 (Fig. 6FF) are relatively buccolingually elongate in proportions, in contrast to the P4 which is approximately mesiodistally long as buccolingually wide. The P1, P3, and P4 have four or five roots, a distinct protocone, paracone, metacone, and hypocone. A small parastyle is present on P1 and P3. The parastyle on P4 (Fig. 6GG) is proportionally much larger and mesiobuccally oriented. The P4 also bears a small, but distinct, mesostyle connected to the metacone and paracone by a pair of peaked crests. The paraconule, metaconule, and mesostyle are absent. The protocone is flanked by both a preprotocrista and postprotocrista. The protocone is approximately buccolingually in line with the paracone.

Two teeth are identified as deciduous premolars (KNM-TP 102147, KNM-TP 102501, Fig. 5H, I). Each has a well-developed hypocone only slightly smaller than the other three main cusps, but is smaller than those on the M1s of this species. They also have a more strongly expressed postprotocrista, and sharper or more gracile cusps compared with upper molars.

Upper Molars—The dentition increases in size from premolars to molars. Increase in crown area along the upper molar row is distinct: the M2 is ~1.1 times the area of the M1, but the M3 ~1.5 times the area of the M1 (Figs. 6HH–KK, 7). Some upper molars have concave mesial margins consistent with interlocking mesial and distal molar walls, though this character varies between specimens. Buccal and lingual cusps are moderately convergent. The distal cusp pair (the hypocone and metacone) are spaced closer to each other than the mesial cusp pair (protocone and paracone) is. Buccal cusps are slightly internalized, such that the paracone is only slightly offset from the buccal margin of the tooth and a buccal cingulum is well-developed. The cingulum traverses the lingual wall of the mesostyle. Entostyles,

metaconules, spurs on the ectoloph, and lingual spurs on the buccal cusps are absent, although there is frequently an expanded lip of enamel on the cingulum where an entostyle might be located.

The cusp of the protocone itself is small, as or less prominent than the preprotocrista and postprotocrista. This pattern of relative size gives the protocone a crestiform appearance. The protocone has a distinct lingual expansion or placement of the cusp relative to the preprotocrista, and it is surrounded on that side by a nearly continuous cingulum. The preprotocrista is oriented buccomesially with respect to the paracone, but neither converges with the paracone nor with the mesial cingulum. A swelling along the preprotocrista is interpreted as a paraconule, weakly developed (Seiffert, 2003). The postprotocrista is present, but weakly expressed. The parastyle is only slightly smaller than the paracone, and is weakly buccally oriented.

The metacone is present and distinct, much larger than associated crests. The postmetacrista is small and distally oriented. The mesostyle is approximately equidistant between the paracone and metacone. It is large, approximately greater than half the area of the paracone. Its placement is relatively close to being in line with the long axis of the tooth row, reducing the expression of a "w" shape among the buccal crests. The hypocone is slightly smaller than the metacone in footprint, but approximately equal to the protocone. A prehypocrista is oriented mesiobuccally and terminated mesial to the metacone. The posthypocrista on the M1 is variably weak or indistinct. The posthypocrista is variably present on the M3 (KNM-TP 102479; Fig. 6JJ). When present, it extends into a low distocrista around the distal margin of the tooth.

Lower Premolars— On lower teeth, all premolar cusps are connected by strong, continuous crests to adjacent cusps. The p1 is double rooted (KNM-TP 102158; Fig. 4R). The trigonid has two cusps, a small paraconid and a large, wide protoconid. On the talonid, a hypoconid is present and its position is variably central or buccal on the crown. A strong cristid obliqua connects either centrally or buccally to a wide postvallid that is inflated around the cristid obliqua on both lingual and buccal sides.

The p2 has at least three roots, if not more (KNM-TP 102130; KMN-TP 102263; Fig. 4S, Y). The tooth position is molarized, with a paraconid, protoconid, metaconid, hypoconid, and entoconid all present. The metaconid and paraconid are slightly smaller than the protoconid. The protoconid and paraconid are connected by a large paracristid. The protoconid and metaconid are connected to each other by a large, complete protocristid. The metaconid is distally expanded along a postmetacristid, but a premetacristid is absent. A cristid obliqua extends from the postvallid between the protocone and metacone to the hypoconid, which then connects to the entoconid through a hypocristid. The entoconid is slightly smaller than the hypoconid. The hypoconid and protoconid are similar in size to one another, with the hypoconid at least half the height of the protoconid.

The p3 has crown morphology similar to the p2, but differs in its larger crown size and distinct presence of a mesiobuccal cingulid as well as a postcingulid (KNM-TP 102526, KNM-TP 102528, Fig. 4T, Z). At approximately the midpoint of the postcingulid is a peak that may correspond to the hypoconulid. Compared with the p2, the p3 has a relatively larger metaconid and entoconid which are similar in size to their buccally placed counterpart cusp. No stylids or cuspules are present.

The topology of the p4 matches that of the p3, but the tooth is larger in overall size (KNM-TP 102526; Fig. 4U). The talonid is narrower than the trigonid. In comparison to the m1, the p4 has a relatively narrower crown and more distally placed metaconid relative to the protoconid. No lower deciduous premolars have yet been recognized.

Lower Molars— Increase in crown area along the lower molar row is substantial: the m2 is ~1.3 times the area of the m1, and the m3 ~1.5 times the area of the m1 (Figs. 4V–AA, 7). The trigonid and talonid are approximately equal in height, but the talonid is longer than the trigonid. Buccolingual pairs of cusps (protoconid-metaconid and hypoconid-entoconid) are offset from one another, such that the lingual cusps, the metaconid and entoconid, are distally offset from their buccal pair. The buccal and lingual molar walls are subvertical, resulting in cusp placement at the periphery of each crown surface. The large size of cristids and lophids in comparison to the size of cusps gives the cusps themselves a more triangular, less conical appearance in occlusal view. This triangular appearance gives the trigonid and talonid basins the appearance of being larger, with walls that excavate into the cusp. Mesoconids, premetacristids, and spurs are absent.

The paracristid of each lower molar is short, continuous and recurved, forming an acute angle with the long axis of the tooth. This relationship is most visible on the m3. No cuspidate paraconid is visible. The metaconid is elevated above the protoconid. The metaconid and protoconid are joined in a tall protocristid. The buccal cingulid is often distinct between the protoconid and hypoconid, and an anterobuccal cingulid is present. Otherwise, buccal cingulids are discontinuous around the crown.

The cristid obliqua ascends the trigonid and terminates between the metaconid and protoconid. The hypoconid and entoconid are distinctly present and cuspidate, although they are connected by a strong hypocristid. The cristid obliqua and the hypocristid meet at the hypoconid at a sharp angle. The entocristid is weakly expressed, if at all, and the entoconid cusp is not expanded mesially, leaving a large, open lingual margin of the talonid basin that is at least half as along as the entoconid itself. On the m1 (KNM-TP 102504, KNM-TP 102464; Fig. 4V, AA) and m2 (KNM-TP 102142; Fig. 4W), the hypoconulid is not a distinct cusp but instead a small, central peak on the postcingulid. The hypoconulid on the m3 is reduced to a small depression with a single cusp at the distobuccal margin of the depression (KNM-TP 102463; Fig. 4X).

Type Locality— Hill 3, Topernawi, Ekitale Basin, west of Lake Turkana, Kenya; stratigraphic unit U4, Topernawi Fm., mid-Oligocene.

Remarks & Comparisons— The specimen chosen as the holotype consists of seven teeth and three indeterminate bone fragments (Figs. 4, S5). Although the individual teeth do not articulate directly with one another, we consider them associated and representative of a single individual for the following reasons. First, they were all recovered in a single, small block of matrix approximately 5 cm in its longest dimension. Individual teeth became separated during preparation of the matrix block. Second, all teeth have similar color and quality of preservation, consistent with a single preservational history. Third, no single element is duplicated, consistent with a single individual (e.g., no duplicate left m3). Fourth, approximate sizes of the teeth relative to one another, including the size of the upper incisor relative to lower molars, are consistent with tooth proportions of other individual hyracoids (Barrow et al., 2012; McKay et al., 2022). Fifth, the relative amount of wear on each tooth is consistent with a single individual. The right and left representatives of the same tooth position (p3) are very similarly worn in both pattern and degree. The p4 is the least worn tooth, the m3 is the next least worn tooth, and the p3 and m1 are comparatively more worn, consistent with an eruption sequence of m1, p1–3, m3, p4 in other hyracoids (Asher et al., 2017).

The pair of species of *Thyrohyrax* from Topernawi (*Thyrohyrax ekaii* and *Thyrohyrax lokutani*) differ from each other in ways that the pair of *Thyrohyrax* from slightly younger sites in Kenya also differ from one another: i.e., *Thyrohyrax kenyaensis* and *Thyrohyrax microdon* from Losodok and Nakwai (Rasmussen & Gutierrez, 2009). Future phylogenetic analyses should incorporate these younger taxa and test more explicitly for the

possibility of direct ancestry between species from Topernawi to Losodok/Nakwai. As the larger of the pair of taxa at Topernawi, *Thyrohyrax lokutani* differs from *Thyrohyrax kenyaensis*, its analog at Losodok/Nakwai, in less frequently having an entostyle; in the valley between the protocone and hypocone being oriented away from the mesial margin of the tooth; in having a more strongly recurved paracristid on the p4; and in having an enclosed trigonid basin on the m2 and m3. It differs from slightly older species from the Fayum, *Thyrohyrax domorictus* (the geologically youngest species of *Thyrohyrax* known from the Fayum), in having a longer, more trapezoidal trigonid on the m1; an even more posteriorly placed entoconid; a smaller parastyle and mesostyle; and a wider cingulum (Meyer, 1973). The premolars of *Thyrohyrax domorictus* are also more molarized with larger hypocones.

The unnamed saghatheriine from Lokone bears some resemblance to *Thyrohyrax lokutani* in its small size, selenodont shape, and a mesostyle equidistant between paracone (Ducrocq et al., 2010). These descriptions of taxa from Topernawi will enable more detailed comparisons between Kenyan taxa in a future study.

Thyrohyrax lokutani differs from *Selenohyrax* and *Saghatherium* in the presence of a well-developed entoconid on the p2, p3, and p4, as well as in having a complete p4 protolophid and hypolophid. On lower molars, *Thyrohyrax lokutani* has a shorter paracristid, a sharp-angled cristid obliqua-hypoconid junction, and a relatively larger entoconid, that is, one that is similar in size to the hypoconid. Correspondingly, on the upper premolars *Thyrohyrax lokutani* has a distinct and well-differentiated metacone on the P1, P2, P3, and P4, as well as a large P4 hypocone and a distinct P4 mesostyle. On the upper molars, it lacks lingual spurs on the M1–2 buccal cusps and buccal "ribs" on the M1–2 centrocrista, as well as a distinct posthypocrista on the M1. Its mesial cingulum on the M1–2 is complete, and it has a more strongly "w"-shaped centrocrista. The buccal and lingual cusps are more widely separated and less internalized. The cusps are, overall, less prominent than the preprotocrista and postprotocrista, giving the region an overall more crestiform appearance than the corresponding region in *Saghatherium* and *Selenohyrax*, which have more prominent cusps.

Thyrohyrax lokutani differs from *Megalohyrax* principally in its much smaller size. It also has more molarized lower premolars, specifically by having a p1–p4 paraconid, a well-developed p2–p4 entoconid, and a complete p4 protolophid and hypolophid. *Thyrohyrax lokutani* also has a p4 much closer in size to the m1. On the lower molars, its paracristid is recurved rather than straight, its cristid obliqua-hypoconid junction is sharp-angled rather than rounded, its entoconid is relatively large and similar in size to the hypoconid, and the m3 hypoconulid is reduced. The protocristid is oblique rather than perpendicular, with the metaconid shifted distally. Upper premolars are also more molarized, specifically in terms of having a distinct, well-differentiated P1–P4 metacone, a hypocone that is present on the P2–P3 and large on the P4, and a mesostyle that is present on the P4. On premolar protocones, *Thyrohyrax lokutani* has spurs of enamel that *Megalohyrax* lacks. On the upper molars, the mesial cingulum is more complete but the M1 posthypocrista is distinct, rather than the trenchant condition in *Megalohyrax*.

THYROHYRAX EKAII sp. nov.
(Figs. 4, 5, and 6; Table 1)

Holotype—KNM-TP 102173, left partial dentary with m1–m3 (Fig. 4KK).

Etymology—Named for Ekai Ekes, who discovered the type specimen.

Referred Specimens—KNM-TP 102083 right p3 and p4, KNM-TP 102121 left maxilla C-P1, KNM-TP 102122 right lower premolar, KNM-TP 102152 left upper premolar, KNM-TP 102159 left maxilla P2–P4, M1, KNM-TP 102166 left m3, KNM-TP 102173 left dentary m1–m3, KNM-TP 102180 right p3, KNM-TP 102194 right M1, KNM-TP 102204 right m3, KNM-TP 102205 right M2, KNM-TP 102218 right m3, KNM-TP 102219 left m1, KNM-TP 102220 left P1, KNM-TP 102223 left M3, KNM-TP 102225 right p2, KNM-TP 102226 left p3, KNM-TP 102229 right dP4?, KNM-TP 102235 left p4, KNM-TP 102237 right m2, KNM-TP 102248 left P4, KNM-TP 102250 left p4, KNM-TP 102254 left M1, KNM-TP 102258 right p3, KNM-TP 102259 right P2 or P3, KNM-TP 102260 right P1, KNM-TP 102261 right dP3 or dP4, KNM-TP 102262 right lower molar, KNM-TP 102456 left m1, KNM-TP 102513 right p1, KNM-TP 102734, right M3, KNM-TP 102868, left M2.

Diagnosis—Diagnosed as *Thyrohyrax* based on apomorphies: small size, molarized premolars with distinct entoconids, selenolophodont cheek teeth with zig-zag lophs. Apomorphies within *Thyrohyrax*: p4 entocristid absent; mesiobuccally inflated, rounded base of hypoconid. Differs from all except *Thyrohyrax microdon:* P3 mesostyle present. Differs from *Thyrohyrax microdon*: more distinct, cuspate metaconid; relatively larger m3; more lingually placed apex of hypocone; mesostyle ending more lingually. Differs from *Thyrohyrax lokutani* and *Thyrohyrax kenyaensis*: metaconid in line with protoconid, entoconid in line with hypoconid, presence of buccally oriented spur on premolar protocone, proportionally shorter molars, relatively smaller upper molar distal cusps, more weakly expressed crests between buccal crown features, valley between protocone and hypocone in line with the mesostyle, M1 distal cusp pairs similarly spaced relative to mesial cusp pairs, more continuous, larger labial cingulum around base of M2 protocone, weaker gradient of size increase along molar row with first and second molars more equally sized, mesostyle closer to metacone than protocone.

Description

Upper Premolars—P1 has four roots (KNM-TP 102220; Fig. 6RR). The P1 crown is multi-cusped with a distinct protocone, paracone, and metacone (KNM-TP 102260; Fig. 6LL). The paracone and metacone are connected by a low, straight crista that continues as a postmetacristid to the distal margin of the crown. A small, distinct parastyle lies directly mesial to the paracone. A precingulum is present and continuous along the mesial margin of the tooth. A preprotocrista extends nearly continuously straight from the protocone to the paracone. No hypocone is apparent. The distal margin of the crown is rounded and expanded far past the distal edge of the metacone, giving the tooth a more rounded appearance overall.

P2 (KNM-TP 102259; Fig. 6MM) has a distinct protocone, paracone, metacone, mesial precingulum, and parastyle. Similar to the P1, it has a connection between the paracone and metacone and no mesostyle between the two cusps. A preprotocrista extends to the base of the paracone and is curved mesially. Short lingual spurs are present on both the paracone and metacone, but do not connect to any other cusp. A wide lingual ridge, potentially a distally directed postprotocrista, extends from the protocone toward a small, weakly expressed hypocone. The distolingual and distobuccal corners of the crown area are expanded, giving the tooth a more rectangular appearance then the P1. This expansion also puts the buccal pair of cusps on a line offset from the buccal margin of the tooth.

The single proposed P4 is highly molarized, with a hypocone similar in size to the other three main cusps and small mesostyle weakly differentiated from the centrocrista (KNM-TP 102248;

Fig. 6NN). The paracone and metacone are in line with each other buccolingually along with a parastyle. One isolated tooth is identified as a deciduous premolar (KNM-TP 102261; Fig. 5J). The tooth has a distinct mesostyle buccally displaced from the paracone and metacone, and a distal cusp pair more closely appressed to one another than are corresponding cusp pairs in upper molars.

Upper Molars—The dentition increases in size from premolars to molars. Increase in crown area along the upper molar row is slight: the M2 is only ~1.2 times the area of the M1, and the M3 only ~1.1 times the area of the M1 (Fig. 6OO–UU; Fig. 7). Teeth are relatively brachydont. Upper teeth are generally quadritubercular.

The mesial cingulum is continuous along the margin of the crown. The lingual cingulum is variable between molar positions, well developed in the M1 and poorly developed in the M3. In general it is present around the protocone and expanded around the emargination between protocone and metacone, providing a straighter lingual outline. The buccal cingulum is narrow and variably continuous along the crown margin. In combination with the presence of cingula, the placement and slopes of cusps make them appear slightly internalized, or offset from the edge of the crown surface. Conules and "ribs" or mesial or lingual spurs, cf. Rasmussen and Simons (1988) and Pickford (2004) are absent.

The lingual face of the protocone is flattened and steeply sloping, neither convex and inflated nor shallowly sloping. The preprotocrista remains separate from the mesial cingulum and parastyle. It ends along the mesial face of the paracone. The postprotocrista is also variably present. Where present, it is usually oriented toward the distolingual border of the crown. The paracone is offset lingually from the buccal margin of the tooth such that almost the entirety of the cusp is located lingual to the parastyle and mesostyle. The parastyle is mesiobuccally oriented, with increasingly buccal orientation in successive tooth loci. A centrocrista extends from the parastyle to the metacone and is W-shaped. Along the centrocrista, the mesostyle is located closer to the metacone than the paracone. The mesostyle is relatively large, with the length of the base of the style at least half the length of the metacone. It becomes a proportionally smaller part of the tooth crown on successive molar loci. The hypocone occupies a larger surface area than the metacone, and is more similar in size to the protocone. The prehypocrista is oriented toward the notch between the paracone and metacone. The posthypocrista is not distinctly present on three out of four upper molars, but is expressed on a fourth (KNM-TP 102194). The cusps are equally or less prominent than the cristae, particularly the preprotocrista and postprotocrista, giving the region an overall crestiform appearance. Entostyles are absent.

The M1 (Fig. 6OO, SS) is approximately as mesiodistally long as it is buccodistally wide, with the four main cusps located approximately equidistant from one another forming a relatively square-shaped crown. Aside from the two characters generally used to assign isolated teeth to M1s, representatives of this tooth position tend to have a premetacrista and weakly developed postmetacrista more directly distally oriented, versus the more distolingual orientation of the pre- and postmetacrista on the M2 (Fig. 6PP, TT). This orientation results in a metacone that appears more compressed on the M1 and more elongate on the M2. The M2 mesostyle is less than half the area of the paracone.

In comparison to the first two molars, the paracone and metacone on the M3 (Fig. 6QQ, UU) is notably inset lingually from the buccal margin. The parastyle is relatively larger and more lingually expanded than in preceding molars but the rest of the cusp defined by the position of the four major cusps retains a relatively equilateral shape. The hypocone and metacone remain relatively transversely, or buccolingually, oriented. The hypocone and posthypocrista on the M3 form a low distocrista.

Lower Premolars—The lower premolar field transitions along its length from a relatively simplified p1 to a molarized p4. The p1 contains only three distinct cusps arranged along a single line. The main cusp is interpreted as the protoconid, with a smaller paraconid anteriorly and a hypoconid posteriorly, connected to the paraconid by a small cristid obliqua. The p2 has a distinct trigonid with three cusps, a small paraconid, a protoconid, and a metaconid. They are arranged in a triangle and connected to each other through a paracristid and protocristid (KNM-TP 102225; Fig. 4CC). The talonid has a distinct hypoconid at least half as tall as the protoconid, with both a cristid obliqua and a posthypocristid. The p2 (Fig. 4DD) has at least three roots, although some are still partially encased in bone and the total number cannot be determined. The p3 has a crown topology similar to the p2, but the crown surface is relatively wider (KNM-TP 102180; Fig. 4EE). The protoconid and metaconid are also less offset from each other mesiodistally than they are on the p2.

The p4 trigonid and talonid are of approximately equal widths (KNM-TP 102250, KNM-TP 102235; Fig. 4FF, JJ). The trigonid retains all three trigonid cusps, among which the paraconid is smaller than the other two. The metaconid and protoconid form a transverse line approximately perpendicular to the long axis of the tooth. A premetacristid is absent. On the talonid there is a distinct entoconid similar in size to the hypoconid. The hypoconid is placed buccally on the tooth, and the two cusps are connected by a complete hypocristid. A strong cristid obliqua extends from the hypoconid to the postvallid, where it terminates between the metaconid and protoconid. The entoconid is mesially expanded, terminating in a preentocristid that partially encloses a talonid basin. No lower deciduous premolars have yet been recognized.

Lower Molars—Increase in crown area along the lower molar row is slight. The m2 is ~1.1 times the area of the m1, and the m3 only ~1.3 times the area of the m1 (Figs. 4GG–II, KK, 7). The trigonid and talonid are similar in height. The talonid is longer than the trigonid. The buccal and lingual molar walls are subvertical with cusps located at or near the margins of the crown. A buccal cingulid is absent. The paraconid is not recognizable as a distinct cusp but a short paracristid is present. It is continuous and unbroken, nearly perpendicular with the long axis of each tooth. The metaconid is elevated above the protoconid. The two are connected by a continuous protocristid. The metaconid is slightly distally offset from the protoconid, although overall the protocristid remains approximately perpendicular to the long axis of the tooth. The premetacristid is weakly expressed or absent, depending on the tooth. Mesoconids and spurs are absent.

The cristid obliqua is variably oriented toward either the metaconid apex or the space between the metaconid and protoconid. The hypoconid and entoconid are paired, distinct cusps in a line with one another perpendicular to the long axis of the tooth. They are connected to one another by a continuous hypocristid. The hypocristid and cristid obliqua together form a 'v' shape with the hypoconid at the vertex. The entoconid is expanded mesially and also bears a small, but distinct entocristid, resulting in a talonid basin that is nearly completely enclosed lingually. The m1 (KNM-TP 102456, KNM-TP 102173; Fig. 5GG, KK) and m2 (KNM-TP 102237, KNM-TP 102173; Fig. 6HH, KK) contain no distinct hypoconulid, but the postcingulid has a small mesial peak. No crest connects the hypoconid and this peak. The hypoconulid on the m3 (KNM-TP 102204, KNM-TP 102173; Fig. 6II, KK) forms a lobe projecting from a relatively flat wall formed by the hypoconid and entoconid. The lobe contains a single, strongly expressed cristid connecting this wall to a distinct hypoconulid cusp on the distobuccal tip of the lobe. The

lingual edge of the lobe is much lower, with no distinct cristid along the margin.

Type Locality— Hill 2, Topernawi, Ekitale Basin, west of Lake Turkana, Kenya; stratigraphic unit U4, Topernawi Fm., mid-Oligocene.

Remarks & Comparisons— As the smaller of the pair of taxa at Topernawi, *Thyrohyrax ekaii* differs from *Thyrohyrax microdon*, its analog at Losodok/Nakwai, in having a more distinct, cuspate metaconid, a relatively larger m3, a more lingually placed apex of the hypocone, and a mesostyle that does not extend as far buccally.

Thyrohyrax ekaii differs from *Thyrohyrax libycus*, a related species from slightly older deposits in Libya, in having a more molarized P4 with a more distinct hypocone, a larger mesostyle, and larger parastyle (Coster et al., 2015). It also differs from the slightly older or contemporaneous species from the Fayum, *Thyrohyrax domorictus*, the geologically youngest species of *Thyrohyrax* known from the Jebel Qatrani Formation, in having a more molarized P2 with a hypocone present, a more elongate M3, lacking a recurved paracristid and buccal cingulum, and having a more anteriorly placed entoconid.

Thyrohyrax ekaii differs from *Saghatherium*, *Selenohyrax*, and *Megalohyrax* in all the ways that *Thyrohyrax lokutani* also differs, with the following exceptions: *Thyrohyrax ekaii* lacks a p2 entoconid and has a smaller p4 relative to the m1, similar to the other genera. It differs in having a mesiobuccally trending prehypocrista on upper molars. It differs from both *Saghatherium* and *Thyrohyrax lokutani* in having a straight, rather than recurved, paracristid and a perpendicular protocristid on lower molars and in lacking spurs on upper premolar protocones.

RESULTS

Phylogenetic Analyses

Choice of character sampling Markov model for the Bayesian tip-dating analysis (correcting for invariant characters observed or not) or burn-in percentage (25% vs. 50%) did not affect tree topology, nor estimated divergence dates, nor posterior probability values by more than 0.02 at any given node, nor ESS relative to the acceptance threshold (>200). We present the 50% consensus tree from the optimal Bayesian tip-dating topology (Mkv-based analysis; Fig. 8). Overall topology is similar to the topology resulting from previous, parsimony-based analyses of a similar matrix (Barrow et al., 2012; Cooper et al., 2014; Seiffert, 2007). The clades Geniohyidae, Titanohyracidae, and *Megalohyrax* are all recovered with high posterior probability (>0.98), as are a clade of *Selenohyrax* + *Saghatherium*. The genera *Nengohyrax*, *Abdahyrax*, and *Geniohyus* are all recovered as members of Geniohyidae, although interrelationships between species are not well supported within the clade. The species *Thyrohyrax lokutani* and *Thyrohyrax ekaii* are both recovered among other species of *Thyrohyrax* in a paraphyletic grade receiving mixed support at various nodes.

The single topology produced by a parsimony analysis with implied weights (Fig. S6) produced largely congruent results with Bayesian analyses, specifically in recovering the clade Geniohyidae including *Geniohyus*, *Nengohyrax*, and *Abdahyrax*, albeit with different interrelationships; a clade Titanohyracidae, again with different interrelationships; and a *Selenohyrax* + *Saghatherium* clade. The two trees differ in the hypothesized relationships of species of *Thyrohyrax*, which is a polyphyletic group ranging widely across the tree resulting from the parsimony analysis.

Body Mass Estimates

Use of upper and lower second molars to estimate body mass of each species produced largely congruent results (Fig. 9, Table 2). Estimates for larger-bodied species based on individual teeth ranged widely, but not systematically by upper vs. lower teeth. The largest hyracoid species at Topernawi, *Nengohyrax josephi*, weighed on average between 130 and 173 kg, comparable to reconstructions for *Titanohyrax angustidens*, *Megalohyrax eocaenus*, *Bunohyrax major*, and *Pachyhyrax crassidentatus* (Schwartz et al., 1995). The smallest species, *Thyrohyrax ekaii*, weighed on average 7.9–11.9 kg, larger than the extant *Procavia capensis* but of the same general size as *Thyrohyrax meyeri* and *Saghatherium bowni*.

DISCUSSION

Hyracoids from Topernawi are a relatively diverse assemblage of five known species, but phylogenetically represent only two clades: Geniohyidae and *Thyrohyrax*. The systematics of extinct Hyracoidea are still unsettled. A long-standing incongruity between traditional systematic organization (Rasmussen & Gutierrez, 2010) and results of phylogenetic analyses remains unresolved (Barrow et al., 2010, 2012; Cooper et al., 2014; Seiffert, 2007).

Geniohyidae is one of the clades that is more stable and consistent between systematic schemes. Our proposed dental apomorphies for this clade may help resolve the situation of Geniohyidae being considered a problematic group of primitive-looking hyracoids (Tabuce et al., 2021). As recognized in this study, without *Seggeurius*, it is a monophyletic group receiving high posterior probability support (Court & Mahboubi, 1993). The same clade is recovered when other analytical models are used, and it received weak bootstrap support and Bremer support (Barrow et al., 2012; Cooper et al., 2014). Its composition is largely consistent with the phenetically recognized concept of Geniohyidae (Rasmussen & Gutierrez, 2010). Within Geniohyidae, relationships between species are not well resolved, which is one of the reasons why we do not assign *Nengohyrax josephi* and *Abdahyrax philipi* to existing genera. Work remains to add other African taxa, especially additional species of *Brachyhyrax*, and better resolve interrelationships between members of the clade.

In contrast, Saghatheriidae, a clade traditionally composed of *Saghatherium*, *Microhyrax*, *Selenohyrax*, *Thyrohyrax*, and *Megalohyrax,* has met with very little phylogenetic support (Barrow et al., 2012; Seiffert, 2007). Even individual genera within Saghatheriidae, principally *Thyrohyrax*, are not resolved as monophyletic groups (Fig. 8; Barrow et al., 2012). *Thyrohyrax* is a morphologically coherent and identifiable set of taxa within faunas. Phylogenetically, it resolves as paraphyletic with respect to Neogene and extant hyracoids (Barrow et al., 2012), although support values for this hypothesized relationship are not high regardless of analysis type (Fig. 8, Barrow et al., 2012; Cooper et al., 2014). The presence of two species of *Thyrohyrax* at Topernawi closely mirrors the two species of *Thyrohyrax* at the younger Kenyan sites of Losodok and Nakwai (Rasmussen & Gutierrez, 2009). The teeth also bear resemblance to the indeterminate sagatheriids at Lokone (Ducrocq et al., 2010). Given the difficulty of assigning isolated incisors to species in an assemblage of multiple hyracoids, it is difficult to compare fossils from Topernawi to those of *Rukwalorax* from Rukwa, Tanzania (Stevens et al., 2009). Future work should more closely investigate potential relationships between these taxa.

Based on the five new hyracoid taxa described here, Topernawi compares favorably to Paleogene communities from Kenya, Ethiopia, Angola, and Egypt in terms of raw hyracoid diversity (Kappelman et al., 2003; Rasmussen & Gutierrez, 2009, 2010;

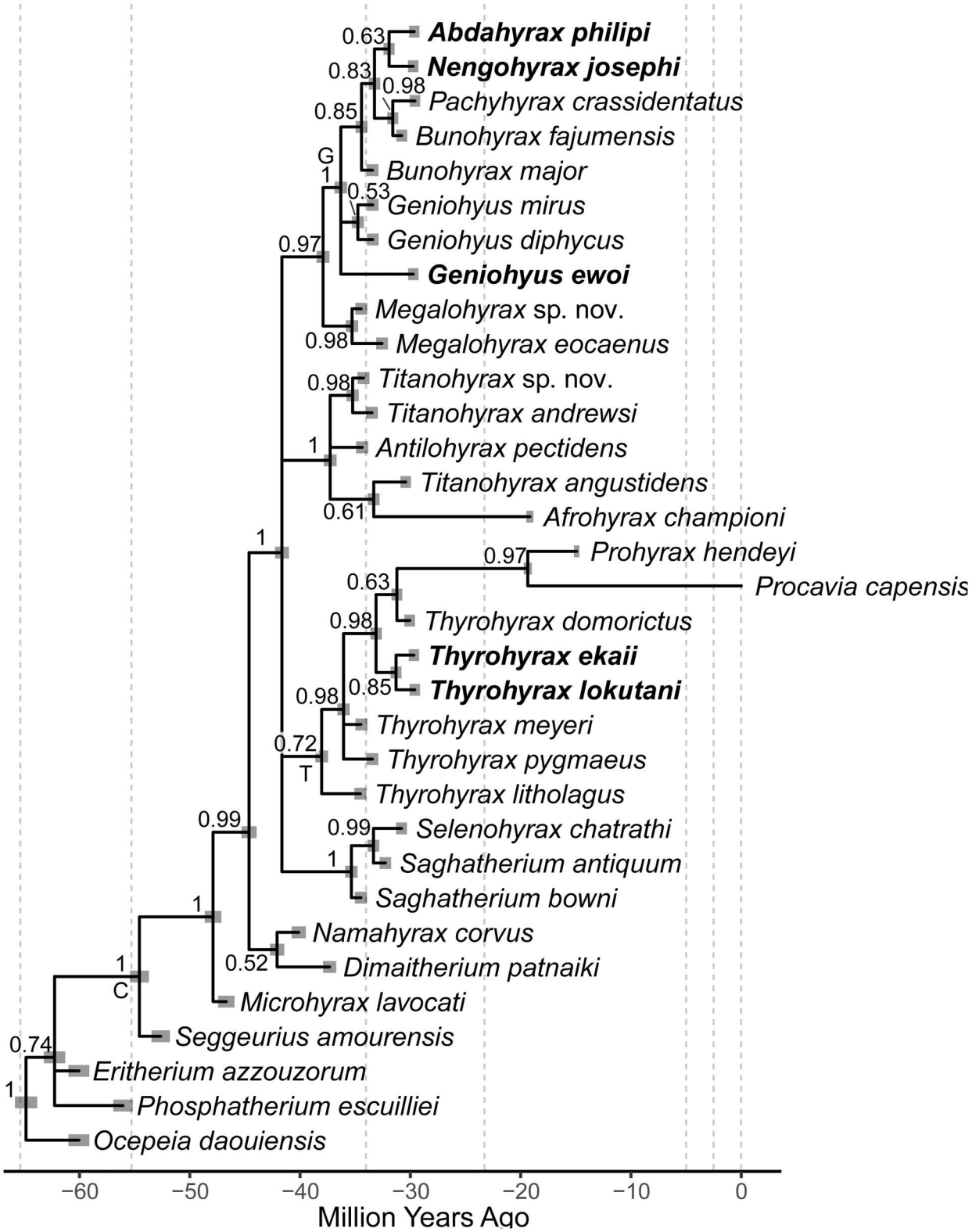

FIGURE 8. Majority rule consensus tree of hyracoid relationships based on Bayesian tip-dated analysis. C indicates the node constrained to enforce outgroup taxa. G indicates clade Geniohyidae. T indicates the note containing *Thyrohyrax* and most closely related taxa. Values at nodes indicate Bayesian posterior probabilities (BPP). Horizontal bars indicate estimated age ranges of nodes and input age ranges of tips. Vertical, dashed gray lines indicate epoch boundaries.

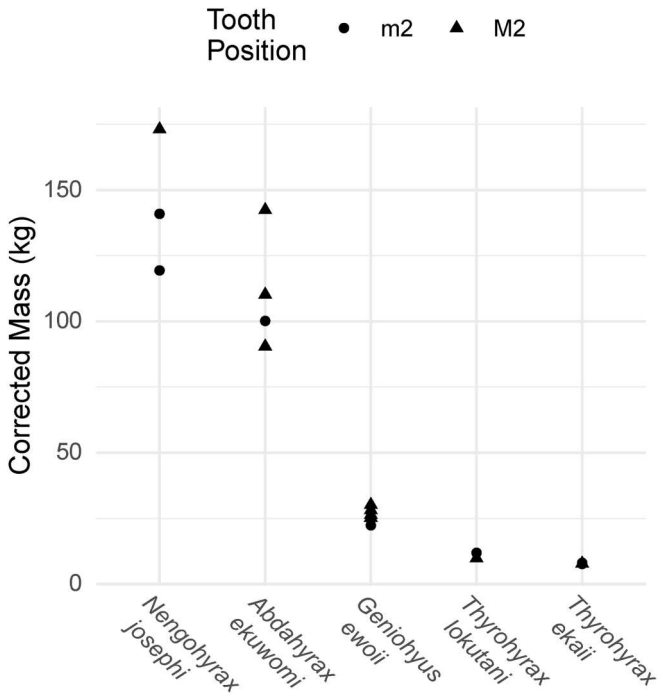

FIGURE 9. Estimated body masses for hyracoids from Topernawi based on lengths of upper and lower second molars.

Tabuce et al., 2021). Those communities all contain 4–6 species of hyracoids occupying a range of body sizes (Schwartz et al., 1995). Unlike the sites of Chilga, Ethiopia, and Malembo, Angola, both small-bodied and large-bodied hyracoids are recovered among the fossils at Topernawi. Compared to Eocene and Oligocene sites at the Fayum quarries, one of the most characteristic missing taxa are any very large species rivaling the largest-bodied (and exceedingly rare) *Titanohyrax ultimus*, which is found at the youngest quarries (I and M) and is reconstructed to be ~1000 kg (Gagnon, 1997; Schwartz et al., 1995). However, in total the body size range at Topernawi is comparable to the rest of body size diversity at other sites, including smaller-bodied members of *Titanohyrax* (Schwartz et al., 1995). Topernawi is also missing some characteristic Neogene or late Paleogene, high-crowned taxa such as *Afrohyrax* and *Meroehyrax* (Rasmussen & Gutierrez, 2009; Whitworth, 1954). All taxa at Topernawi qualitatively have relatively brachydont, low-crowned teeth. More detailed analyses of diversity, including functional analyses, are beyond the scope of this descriptive study, but are a line of ongoing research.

Lower molar proportions in both clades are similar to the prediction of the inhibitory cascade model, as was also found for other species of *Throhyrax* and extant hyracoids in previous studies (Kavanagh et al., 2007; McKay et al., 2022; Polly, 2007). Hyracoids in general are conservative in having lower molars that increase in size down the tooth row (Vitek & Princehouse, 2024), and it may be that they are a clade that hews closely to the specific predictions of the inhibitory cascade model, although further statistical tests are needed.

Overall, these new taxa support the traditional characterization of hyracoids as being major components of Paleogene African faunas (Gagnon, 1997; Rasmussen, 1989). Some taxonomic similarity at higher levels belies the observation that there is significant turnover between sites that remains unexplained. The continued discovery of new taxa with each new site also suggests that much of hyracoid diversity on the continent still remains to be found.

TABLE 2. Mean of individual specimen-based estimates of body masses for hyracoids from Topernawi.

Species	Tooth	Mean estimated body mass (kg)
Nengohyrax josephi	m2	130.2
Nengohyrax josephi	M2	173.1
Abdahyrax philipi	m2	100.2
Abdahyrax philipi	M2	114.3
Geniohyus ewoi	m2	22.4
Geniohyus ewoi	M2	27.5
Thyrohyrax lokutani	m2	11.9
Thyrohyrax lokutani	M2	9.8
Thyrohyrax ekaii	m2	7.9
Thyrohyrax ekaii	M2	7.9

DISCLOSURE STATEMENT

No potential conflict of interest was reported by the author(s).

DATA AVAILABILITY STATEMENT

A Mesquite-readable nexus file including taxa, character scorings, character state descriptions, and decisions about character ordering is included in Supplemental Data. An online-accessible version of the NEXUS file is hosted on MorphoBank under project P4786 (http://morphobank.org/permalink/?P4786). New measurements are presented in Table 1 of the main text. Other, previously published measurements can be found in the sources cited in text. Scripts used to conduct analyses and summarize results are reposited in an associated project on Dryad (DOI: 10.5061/dryad.2jm63xsw2).

SUPPLEMENTARY FILES

Supplemental Data 1.docx: Supplemental Tables S1–3, and Figs. S1–6.

AUTHOR CONTRIBUTIONS

PMP, FJS, ION, and NSV led fieldwork, primarily led by head of project PMP and with participation from ERS, MWG, CSF, FJS, EEA. MWG and CSF led field mapping of fossils, with support from EEA and FJS. FJS conducted field stratigraphic work. ERS and SH provided critical input and data for phylogenetic analyses, and ERS provided discussion and feedback about identifications. NSV conducted primary identification and description of the fossils, conducted phylogenetic analyses and other statistical analyses, and drafted the manuscript. All authors edited the manuscript.

ACKNOWLEDGMENTS

Thanks to collections staff at the AMNH, DLCMNH, KNM, and YPM, including J. Meng, J. Galkan, M. Borths, C. Riddle, F.K. Manthi, J. Kibii, P. Mbete, J. Yatich, S. Maikweki, V. Rhue, D. Brinkman, for assistance with specimens in their care; to R. Muthoni and T. Gichunge for digitizing specimens from Topernawi; S. Ducrocq for making casts of Lokone material for comparison; to the Turkana Basin Institute for logistical and infrastructure support during fieldwork; to the many members of the Topernawi Research Project field crews; funding from NSF BCS-2124790, 2124791, 2124792, DBI-2023087 EAR-2021682. The Turkana Miocene Project is acknowledged for logistical assistance; NACOSTI permit numbers: P/21/8274, P/22/16127, P/23/641, P/23/29752. This is TMP publication #3 and Duke Lemur Center publication #1599.

ORCID

Natasha S. Vitek http://orcid.org/0000-0003-0587-8907

LITERATURE CITED

Andrews, C. W. (1906). A Descriptive Catalogue of the Tertiary Vertebrata of the Fayûm, Egypt. Based on the Collection of the Egyptian Government in the Geological Museum, Cairo, and on the Collection in the British Museum (Natural History), London. Printed by order of the Trustees of the British Museum, London, 324 pp.

Asher, R. J., Gunnell, G. F., Seiffert, E. R., Pattinson, D., Tabuce, R., Hautier, L., & Sallam, H. M. (2017). Dental eruption and growth in Hyracoidea (Mammalia, Afrotheria). *Journal of Vertebrate Paleontology*, *37*(3), e1317638. https://doi.org/10.1080/02724634.2017.1317638

Baczynski, A. A., McInerney, F. A., Wing, S. L., Kraus, M. J., Morse, P. E., Bloch, J. I., Chung, A. H., & Freeman, K. H. (2016). Distortion of carbon isotope excursion in bulk soil organic matter during the Paleocene-Eocene thermal maximum. *Geological Society of America Bulletin*, *128*(9-10), 1352–1366. https://doi.org/10.1130/B31389.1

Barido-Sottani, J., Saupe, E. E., Smiley, T. M., Soul, L. C., Wright, A. M., & Warnock, R. C. M. (2020). Seven rules for simulations in paleobiology. *Paleobiology*, 1–10. https://doi.org/10.1017/pab.2020.30

Barrow, E. C., Seiffert, E. R., & Simons, E. L. (2010). A primitive hyracoid (Mammalia, Paenungulata) from the early Priabonian (Late Eocene) of Egypt. *Journal of Systematic Palaeontology*, *8*(2), 213–244. https://doi.org/10.1080/14772010903450407

Barrow, E. C., Seiffert, E. R., & Simons, E. L. (2012). Cranial morphology of *Thyrohyrax domorictus* (Mammalia, Hyracoidea) from the early Oligocene of Egypt. *Journal of Vertebrate Paleontology*, *32*(1), 166–179. https://doi.org/10.1080/02724634.2012.635735

Behrensmeyer, A. K. (1975). The taphonomy and paleoecology of Plio-Pleistocene vertebrate assemblages east of Lake Rudolf, Kenya. *Bulletin of the Museum of Comparative Zoology*, *146*(10), 473–578.

Benoit, J., Crochet, J.-Y., Mahboubi, M., Jaeger, J.-J., Bensalah, M., Adaci, M., & Tabuce, R. (2016). New material of *Seggeurius amourensis* (Paenungulata, Hyracoidea), including a partial skull with intact basicranium. *Journal of Vertebrate Paleontology*, *36*(1), e1034358. https://doi.org/10.1080/02724634.2015.1034358

Butler, P. M. (1939). Studies of the mammalian dentition.–Differentiation of the post-canine dentition. *Proceedings of the Zoological Society of London*, *109*(1), 1–36. doi:10.1111/j.1469-7998.1939.tb00021.x

Cooper, L. N., Seiffert, E. R., Clementz, M., Madar, S. I., Bajpai, S., Hussain, S. T., & Thewissen, J. G. M. (2014). Anthracobunids from the Middle Eocene of India and Pakistan are stem perissodactyls. *PLoS ONE*, *9*(10), e109232. https://doi.org/10.1371/journal.pone.0109232

Coster, P. M. C., Beard, K. C., Salem, M. J., Chaimanee, Y., Brunet, M., & Jaeger, J.-J. (2015). A new early Oligocene mammal fauna from the Sirt Basin, central Libya: Biostratigraphic and paleobiogeographic implications. *Journal of African Earth Sciences*, *104*, 43–55. https://doi.org/10.1016/j.jafrearsci.2015.01.006

Coster, P. M. C., Benammi, M., Mahboubi, M., Tabuce, R., Adaci, M., Marivaux, L., Bensalah, M., Mahboubi, S., Mahboubi, A., Mebrouk, F., Maameri, C., & Jaeger, J.-J. (2012). Chronology of the Eocene continental deposits of Africa: Magnetostratigraphy and biostratigraphy of the El Kohol and Glib Zegdou Formations, Algeria. *Geological Society of America Bulletin*, *124*(9–10), 1590–1606. https://doi.org/10.1130/B30565.1

Cote, S., Kingston, J., Deino, A., Winkler, A., Kityo, R., & MacLatchy, L. (2018). Evidence for rapid faunal change in the early Miocene of East Africa based on revised biostratigraphic and radiometric dating of Bukwa, Uganda. *Journal of Human Evolution*, *116*, 95–107. https://doi.org/10.1016/j.jhevol.2017.12.001

Court, N., & Hartenberger, J.-L. (1992). A new species of the hyracoid mammal *Titanohyrax* from the Eocene of Tunisia. *Palaeontology*, *35*(2), 309–317.

Court, N., & Mahboubi, M. (1993). Reassessment of Lower Eocene *Seggeurius amourensis*: aspects of primitive dental morphology in the mammalian order Hyracoidea. *Journal of Paleontology*, *67*(5), 889–893. https://doi.org/10.1017/S002233600003715X

Crompton, A. W., & Hiiemae, K. (1970). Molar occlusion and mandibular movements during occlusion in the American opossum, *Didelphis marsupialis* L. *Zoological Journal of the Linnean Society*, *49*(1), 21–47. https://doi.org/10.1111/j.1096-3642.1970.tb00728.x

De Blieux, D. D., & Simons, E. L. (2002). Cranial and dental anatomy of *Antilohyrax pectidens:* a Late Eocene hyracoid (Mammalia) from the Fayum, Egypt. *Journal of Vertebrate Paleontology*, *22*(1), 122–136. https://doi.org/10.1671/0272-4634(2002)022[0122:CADAOA]2.0.CO;2

Drake, R. E., Van Couvering, J. A., Pickford, M. H., Curtis, G. H., & Harris, J. A. (1988). New chronology for the Early Miocene mammalian faunas of Kisingiri, Western Kenya. *Journal of the Geological Society*, *145*(3), 479–491. https://doi.org/10.1144/gsjgs.145.3.0479

Drummond, A. J., Ho, S. Y. W., Phillips, M. J., & Rambaut, A. (2006). Relaxed phylogenetics and dating with confidence. *PLoS Biology*, *4*(5), e88. https://doi.org/10.1371/journal.pbio.0040088

Ducrocq, S., Boisserie, J.-R., Tiercelin, J.-J., Delmer, C., Garcia, G., Kyalo, M. F., Leakey, M. G., Marivaux, L., Otero, O., Peigné, S., Tassy, P., & Lihoreau, F. (2010). New Oligocene vertebrate localities from Northern Kenya (Turkana basin). *Journal of Vertebrate Paleontology*, *30*(1), 293–299. https://doi.org/10.1080/02724630903413065

Feibel, C. S., & Brown, F. H. (1991). Age of the primate-bearing deposits on Maboko Island, Kenya. *Journal of Human Evolution*, *21*(3), 221–225. https://doi.org/10.1016/0047-2484(91)90063-2

Gagnon, M. (1997). Ecological diversity and community ecology in the Fayum sequence (Egypt). *Journal of Human Evolution*, *32*(2–3), 133–160. https://doi.org/10.1006/jhev.1996.0107

Gavryushkina, A., Heath, T. A., Ksepka, D. T., Stadler, T., Welch, D., & Drummond, A. J. (2016). Bayesian total-evidence dating reveals the recent crown radiation of penguins. *Systematic Biology*, *66*(1), 57–73. https://doi.org/10.1093/sysbio/syw060

Gheerbrant, E. (2009). Paleocene emergence of elephant relatives and the rapid radiation of African ungulates. *Proceedings of the National Academy of Sciences*, *106*(26), 10717–10721. https://doi.org/10.1073/pnas.0900251106

Gheerbrant, E., Amaghzaz, M., Bouya, B., Goussard, F., & Letenneur, C. (2014). *Ocepeia* (Middle Paleocene of Morocco): The oldest skull of an afrotherian mammal. *PLoS ONE*, *9*(2), e89739. https://doi.org/10.1371/journal.pone.0089739

Gheerbrant, E., Sudre, J., Tassy, P., Amaghzaz, M., Bouya, B., & Iarochène, M. (2005). Nouvelles données sur *Phosphatherium escuilliei* (Mammalia, Proboscidea) de l'Éocène inférieur du Maroc, apports à la phylogénie des Proboscidea et des ongulés lophodontes. *Geodiversitas*, *27*(2), 239–333.

Goloboff, P. A., & Catalano, S. A. (2016). TNT version 1.5, including a full implementation of phylogenetic morphometrics. *Cladistics*, *32*(3), 221–238. https://doi.org/10.1111/cla.12160

Heath, T. A., Huelsenbeck, J. P., & Stadler, T. (2014). The fossilized birth–death process for coherent calibration of divergence-time estimates. *Proceedings of the National Academy of Sciences*, *111*(29), https://doi.org/10.1073/pnas.1319091111

Heritage, S., & Seiffert, E. R. (2022). Total evidence time-scaled phylogenetic and biogeographic models for the evolution of sea cows (Sirenia, Afrotheria). *PeerJ*, *10*, e13886. https://doi.org/10.7717/peerj.13886

Heritage, S., Seiffert, E. R., & Borths, M. R. (2021). Recommended fossil calibrators for time-scaled molecular phylogenies of Afrotheria. *Afrotherian Conservation*, *17*, 1–8.

Hlusko, L. J., Schmitt, C. A., Monson, T. A., Brasil, M. F., & Mahaney, M. C. (2016). The integration of quantitative genetics, paleontology, and neontology reveals genetic underpinnings of primate dental evolution. *Proceedings of the National Academy of Sciences*, 201605901.

Hoeck, H. (2011). Family Procaviidae (Hyraxes). In D. E. Wilson, & R. A. Mittermeier (Eds.), *Handbook of the Mammals of the World: Vol. Volume 2* (pp. 886). Lynx Edicions.

Huxley, T. H. (1869). *An introduction to the classification of animals*. J. Churchill & sons.

IUCN. (2022). *The IUCN Red List of Threatened Species. Version 2022-2*. https://www.iucnredlist.org.

Janis, C. M. (1990). Correlation of cranial and dental variables with body size in ungulates and macropodids. In J. Damuth, & B. J. MacFadden (Eds.), *Body Size in Mammalian Paleobiology: Estimation and Biological Implications* (pp. 255–299). Cambridge University Press.

Kappelman, J., Tab Rasmussen, D. T., Sanders, W. J., Feseha, M., Bown, T., Copeland, P., Crabaugh, J., Fleagle, J., Glantz, M., Gordon, A., Jacobs, B., Maga, M., Muldoon, K., Pan, A., Pyne, L., Richmond, B., Ryan, T., Seiffert, E. R., Sen, S., … Winkler, A. (2003). Oligocene mammals from Ethiopia and faunal exchange between Afro-Arabia and Eurasia. *Nature*, *426*(6966), 549–552. https://doi.org/10.1038/nature02102

Kavanagh, K. D., Evans, A. R., & Jernvall, J. (2007). Predicting evolutionary patterns of mammalian teeth from development. *Nature*, *449* (7161), 427–432. https://doi.org/10.1038/nature06153

Kocsis, L., Gheerbrant, E., Mouflih, M., Cappetta, H., Yans, J., & Amaghzaz, M. (2014). Comprehensive stable isotope investigation of marine biogenic apatite from the late Cretaceous–early Eocene phosphate series of Morocco. *Palaeogeography, Palaeoclimatology, Palaeoecology*, *394*, 74–88. https://doi.org/10.1016/j.palaeo.2013.11.002

Koh, C., Bates, E., Broughton, E., Do, N. T., Fletcher, Z., Mahaney, M. C., & Hlusko, L. J. (2010). Genetic integration of molar cusp size variation in baboons. *American Journal of Physical Anthropology*, *142* (2), 246–260. https://doi.org/10.1002/ajpa.21221

Leakey, M., Grossman, A., Gutiérrez, M., & Fleagle, J. G. (2011). Faunal Change in the Turkana Basin during the Late Oligocene and Miocene. *Evolutionary Anthropology: Issues, News, and Reviews*, *20*(6), 238–253. https://doi.org/10.1002/evan.20338

Lewis, P. O. (2001). A likelihood approach to estimating phylogeny from discrete morphological character data. *Systematic Biology*, *50*(6), 913–925. doi:10.1080/106351501753462876

Linnaeus, C. 1758. Systema Naturae per Regna Tria Naturae: Secundum Classes, Ordines, Genera, Species, Cum Characteribus, Differentiis, Synonymis, Locis, 10th ed. Impensis Direct. Laurentii Salvii, Holmiae, pp.

Lukens, W. E., Lehmann, T., Peppe, D. J., Fox, D. L., Driese, S. G., & Mcnulty, K. P. (2017). The early Miocene Critical Zone at Karungu, western Kenya: an equatorial, open habitat with few primate remains. *Frontiers in Earth Science*, *5*, 21. https://doi.org/doi: 10.3389feart.2017.00087

Maddison, W. P., & Maddison, D. R. (2021). *Mesquite: a modular system for evolutionary analysis* (Version 3.70). http://www.mesquiteproject.org.

Mahboubi, M., Ameur, R., Crochet, J. Y., & Jaeger, J. J. (1986). El Kohol (Saharan Atlas, Algeria): a new Eocene mammal locality in northwestern Africa. *Palaeontographica Abteilung A*, *A192*(1–3), 15–49.

Marshall, P. M. & Butler, P. M. (1966). Molar cusp development in the bat, *Hipposideros beatus*, with reference to the ontogenetic basis of occlusion. *Archives of Oral Biology*, *11*(10), 949-IN1. https://doi.org/10.1016/0003-9969(66)90197-X

Matsumoto, H. (1921). *Megalohyrax* Andrews and *Titanohyrax*, g.n.–A revision of the genera of hyracoids from the Fayûm, Egypt. *Proceedings of the Zoological Society of London*, *91*(4), 839–850. doi:10.1111/j.1096-3642.1921.tb03293.x

Matsumoto, H. (1926). Contribution to the knowledge of the fossil Hyracoidea of the Fayûm, Egypt, with description of several new species. *Bulletin of the American Museum of Natural History*, *56*, 253–350.

McKay, C. J., Welbourn-Green, C., Seiffert, E. R., Sallam, H., Li, J., Kakarala, S. E., Bennett, N. C., & Asher, R. J. (2022). Dental development and first premolar homology in placental mammals. *Vertebrate Zoology*, *72*, 201–218. https://doi.org/10.3897/vz.72.e78234

Meyer, G. E. (1973). A new Oligocene hyrax from the Jebel el Quatrani Formation, Fayum, Egypt. *Postilla*, *163*, 1–11.

Michel, L. A., Lehmann, T., Mcnulty, K. P., Driese, S. G., Dunsworth, H., Fox, D. L., Harcourt-Smith, W. E. H., Jenkins, K., & Peppe, D. J. (2020). Sedimentological and palaeoenvironmental study from Waregi Hill in the Hiwegi Formation (early Miocene) on Rusinga Island, Lake Victoria, Kenya. *Sedimentology*, *67*(7), 3567–3594. https://doi.org/10.1111/sed.12762

Moore, J. R., & Norman, D. B. (2009). Quantitatively evaluating the sources of taphonomic biasing of skeletal element abundances in fossil assemblages. *PALAIOS*, *24*(9), 591–602. https://doi.org/10.2110/palo.2008.p08-135r

Novacek, M. J., Bown, T. M., & Schankler, D. (1985). On the classification of the early Tertiary Erinaceomorpha (Insectivora, Mammalia). *American Museum Novitates*, *2813*, 1–22.

Oates, J. F., Woodman, N., Gaubert, P., Sargis, E. J., Wiafe, E. D., Lecompte, E., Dowsett-Lemaire, F., Dowsett, R. J., Gonedelé Bi, S., Ikemeh, R. A., Djagoun, C. A. M. S., Tomsett, L., & Bearder, S. K. (2022). A new species of tree hyrax (Procaviidae: *Dendrohyrax*) from West Africa and the significance of the Niger–Volta interfluvium in mammalian biogeography. *Zoological Journal of the Linnean Society*, *194*(2), 527–552. https://doi.org/10.1093/zoolinnean/zlab029

Pickford, M. (1994). A new species of *Prohyrax* (Mammalia, Hyracoidea) from the middle Miocene of Arrisdrift, Namibia. *Communications of the Geological Survey of Namibia*, *9*, 43–62.

Pickford, M. (2004). Revision of the Early Miocene Hyracoidea (Mammalia) of East Africa. *Comptes Rendus Palevol*, *3*(8), 675–690. https://doi.org/10.1016/j.crpv.2004.09.002

Pickford, M. (2009). New Neogene hyracoid specimens from the Peri-Tethys region and East Africa. *Paleontological Research*, *13*(3), 265–278. https://doi.org/10.2517/1342-8144-13.3.265

Pickford, M. (2019). Mandible of *Namahyrax corvus* from the Eocene Black Crow Limestone, Namibia. *Communications of the Geological Survey of Namibia*, *21*, 32–39.

Pickford, M., Senut, B., Morales, J., Mein, P., & Sanchez, I. M. (2008). Mammalia from the Lutetian of Namibia. *Memoirs of the Geological Survey of Namibia*, *20*, 465–514.

Polly, P. D. (2007). Development with a bite. *Nature*, *449*(7161), 413–415. doi:10.1038/449413a

Rage, J. C., & Gheerbrant, E. (2020). Island Africa and vertebrate evolution: a review of data and working hypotheses. In G. V. R. Prasad, & R. Patnaik (Eds.), *Biological consequences of Plate tectonics: New perspectives on Post-Gondwana break-up. A tribute to Ashok Sahni* (pp. 251–264.

Ragon, T., Nutz, A., Schuster, M., Ghienne, J., Ruffet, G., & Rubino, J. (2019). Evolution of the northern Turkana Depression (East African Rift System, Kenya) during the Cenozoic rifting: New insights from the Ekitale Basin (28-25.5 Ma). *Geological Journal*, *54*(6), 3468–3488. https://doi.org/10.1002/gj.3339

Rambaut, A., Drummond, A. J., Xie, D., Baele, G., & Suchard, M. A. (2018). Posterior summarization in Bayesian phylogenetics using Tracer 1.7. *Systematic Biology*, *67*(5), 901–904. https://doi.org/10.1093/sysbio/syy032

Rasmussen, D. T. (1989). The evolution of the Hyracoidea: a review of the fossil evidence. In D. R. Prothero, & R. M. Schoch (Eds.), *The Evolution of Perissodactyls* (pp. 57–78). Oxford University Press.

Rasmussen, D. T., Gagnon, M., & Simons, E. L. (1990). Taxeopody in the carpus and tarsus of Oligocene Pliohyracidae (Mammalia: Hyracoidea) and the phyletic position of hyraxes. *Proceedings of the National Academy of Sciences*, *87*(12), 4688–4691. https://doi.org/10.1073/pnas.87.12.4688

Rasmussen, D. T., & Gutierrez, M. (2009). A mammalian fauna from the late Oligocene of northwestern Kenya. *Palaeontographica Abteilung A*, *288*(1–3), 1–52. https://doi.org/10.1127/pala/288/2009/1

Rasmussen, D. T., & Gutierrez, M. (2010). Hyracoidea. In L. Werdelin, & W. J. Sanders (Eds.), *Cenozoic Mammals of Africa* (pp. 123–146). University of California Press.

Rasmussen, D. T., & Simons, E. L. (1988). New Oligocene hyracoids from Egypt. *Journal of Vertebrate Paleontology*, *8*(1), 67–83. https://doi.org/10.1080/02724634.1988.10011684

Rasmussen, D. T., & Simons, E. L. (1991). The oldest Egyptian hyracoids (Mammalia: Pliohyracidae): New species of *Saghatheriums* and *Thyrohyrax* from the Fayum. *Neues Jahrbuch für Geologie und Paläontologie - Abhandlungen*, *182*(2), 187–209. https://doi.org/10.1127/njgpa/182/1991/187

Rasmussen, D. T., & Simons, E. L. (2000). Ecomorphological diversity among Paleogene hyracoids (Mammalia): a new cursorial browser from the Fayum, Egypt. *Journal of Vertebrate Paleontology*, *20*(1), 167–176. https://doi.org/10.1671/0272-4634(2000)020[0167:EDAPHM]2.0.CO;2

Ronquist, F., Teslenko, M., van der Mark, P., Ayres, D. L., Darling, A., Höhna, S., Larget, B., Liu, L., Suchard, M. a., & Huelsenbeck, J. P. (2012). MrBayes 3.2: efficient Bayesian phylogenetic inference and model choice across a large model space. *Systematic Biology*, *61*(3), 539–542. https://doi.org/10.1093/sysbio/sys029

Schmidt-Nielsen, K. (1984). *Scaling: Why is animal size so important?* Cambridge University Press.

Schwartz, G. T., Rasmussen, D. T., & Smith, R. J. (1995). Body-size diversity and community structure of fossil hyracoids. *Journal of Mammalogy*, *76*(4), 1088–1099. https://doi.org/10.2307/1382601

Seiffert, E. R. (2003). *A phylogenetic analysis of living and extinct afrotherian placentals* [PhD Dissertation]. Duke University.

Seiffert, E. R. (2006). Revised age estimates for the later Paleogene mammal faunas of Egypt and Oman. *Proceedings of the National Academy of Sciences*, *103*(13), 5000–5005. https://doi.org/10.1073/pnas.0600689103

Seiffert, E. R. (2007). A new estimate of afrotherian phylogeny based on simultaneous analysis of genomic, morphological, and fossil evidence. *BMC Evolutionary Biology*, *7*(1), 224. https://doi.org/10.1186/1471-2148-7-224

Seiffert, E. R., Nasir, S., Al-Harthy, A., Groenke, J. R., Kraatz, B. P., Stevens, N. J., & Al-Sayigh, A. R. (2012). Diversity in the later Paleogene proboscidean radiation: a small barytheriid from the Oligocene of Dhofar Governorate, Sultanate of Oman. *Naturwissenschaften*, *99*(2), 133–141. https://doi.org/10.1007/s00114-011-0878-9

Smith, M. R. (2019). Bayesian and parsimony approaches reconstruct informative trees from simulated morphological datasets. *Biology Letters*, *15*(2), 20180632. https://doi.org/10.1098/rsbl.2018.0632

Smith, R. J. (1993). Logarithmic transformation bias in allometry. *American Journal of Physical Anthropology*, *90*(2), 215–228. https://doi.org/10.1002/ajpa.1330900208

Sousa, F. J., Cox, S. E., Hemming, S. R., Rasbury, E. T., Steponaitis, E., Hatton, K., Saslaw, M., Henkes, G., Princehouse, P., Vitek, N. S., & Nengo, I. (2022). New discovery of Oligocene strata in the Topernawi Formation, Turkana County, Kenya. *Frontiers in Earth Science*, *10*, 799097. https://doi.org/10.3389/feart.2022.799097

Stanhope, M. J., Waddell, V. G., Madsen, O., De Jong, W., Hedges, S. B., Cleven, G. C., Kao, D., & Springer, M. S. (1998). Molecular evidence for multiple origins of Insectivora and for a new order of endemic African insectivore mammals. *Proceedings of the National Academy of Sciences*, *95*(17), 9967–9972. doi:10.1073/pnas.95.17.9967

Stevens, N. J., O'Connor, P. M., Roberts, E. M., & Gottfried, M. D. (2009). A hyracoid from the Late Oligocene Red Sandstone Group of Tanzania, *Rukwalorax jinokitana* (gen. and sp. nov.). *Journal of Vertebrate Paleontology*, *29*(3), 972–975. https://doi.org/10.1671/039.029.0302

Sudre, J. (1979). Nouveaux mammifered Eocenes du Sahara occidental. *Palaeovertebrata*, *9*(3), 83–115.

Tabuce, R. (2016). A mandible of the hyracoid mammal *Titanohyrax andrewsi* in the collections of the Muséum National d'Histoire Naturelle, Paris (France) with a reassessment of the species. *Palaeovertebrata*, *40*(1), e4. https://doi.org/10.18563/pv.40.1.e4

Tabuce, R., & Benoit, J. (2014). A re-evaluation of *Microhyrax lavocati*: implications for the early radiation of the order Hyracoidea (Mammalia, Afrotheria). *Journal of Vertebrate Paleontology, Program and Abstracts*, *238*.

Tabuce, R., Lihoreau, F., Mees, F., Orliac, M. J., De Putter, T. & Smith, T. (2021). A reassessment of the Oligocene hyracoid mammals from Malembo, Cabinda, Angola. *Geobios*, S0016699521000267. https://doi.org/10.1016/j.geobios.2021.03.003

Tabuce, R., Mahboubi, M., & Sudre, J. (2001). Reassessment of the Algerian Eocene hyracoid *Microhyrax*. Consequences on the early diversity and basal phylogeny of the Order Hyracoidea (Mammalia). *Eclogae Geologicae Helvetiae*, *94*, 537–545.

Thewissen, J. G. M., & Simons, E. L. (2001). Skull of *Megalohyrax eocaenus* (Hyracoidea, Mammalia) from the Oligocene of Egypt. *Journal of Vertebrate Paleontology*, *21*(1), 98–106. https://doi.org/10.1671/0272-4634(2001)021[0098:SOMEHM]2.0.CO;2

Thomas, H., Gheerbrant, E., & Pacaud, J.-M. (2004). Découverte de squelettes subcomplets de mammifères (Hyracoidea) dans le Paléogène d'Afrique (Libye). *Comptes Rendus Palevol*, *3*(3), 209–217. https://doi.org/10.1016/j.crpv.2003.12.004

Tsujikawa, H., & Pickford, M. (2006). Additional specimens of Hyracoidea (Mammalia) from the Early and Middle Miocene of Kenya. *Annales de Paléontologie*, *92*(1), 1–12. https://doi.org/10.1016/j.annpal.2005.11.001

Vitek, N., & Princehouse, P. (2024). Evaluating the utility of linear measurements to identify isolated tooth loci of extinct Hyracoidea. *Acta Palaeontologica Polonica*, *69*, https://doi.org/10.4202/app.01094.2023

Walker, J. D., Geissman, J. W., Bowring, S. A. & Babcock, L. E. (2019). *GSA Geologic Time Scale v. 5.0*. Geological Society of America. https://doi.org/10.1130/2018.CTS005R3C

Wang, L.-G., Lam, T. T.-Y., Xu, S., Dai, Z., Zhou, L., Feng, T., Guo, P., Dunn, C. W., Jones, B. R., Bradley, T., Zhu, H., Guan, Y., Jiang, Y. & Yu, G. (2020). Treeio: an R package for phylogenetic tree input and output with richly annotated and associated data. *Molecular Biology and Evolution*, *37*(2), 599–603. https://doi.org/10.1093/molbev/msz240

Whitworth, T. (1954). The Miocene hyracoids of East Africa, with some observations on the order Hyracoidea. *Fossil Mammals of Africa*, *7*, 1–58.

Yans, J., Amaghzaz, M., Bouya, B., Cappetta, H., Iacumin, P., Kocsis, L., Mouflih, M., Selloum, O., Sen, S., Storme, J.-Y., & Gheerbrant, E. (2014). First carbon isotope chemostratigraphy of the Ouled Abdoun phosphate Basin, Morocco; implications for dating and evolution of earliest African placental mammals. *Gondwana Research*, *25*(1), 257–269. https://doi.org/10.1016/j.gr.2013.04.004

Yu, G. (2022). *Data Integration, Manipulation and Visualization of Phylogenetic Trees* (1st ed.). Chapman and Hall/CRC. https://doi.org/10.1201/9781003279242

Zhang, C., Stadler, T., Klopfstein, S., Heath, T. A., & Ronquist, F. (2016). Total-evidence dating under the fossilized birth–death process. *Systematic Biology*, *65*(2), 228–249. https://doi.org/10.1093/sysbio/syv080

Handling Editor: Julie Meachen.
Phylogenetics Editor: Pedro Godoy.